A quantitative approach to assess histopathological changes in the trachea of dogs and pigs infected with Influenza Virus using an *ex vivo* organ culture system

Thesis submitted in fulfilment of the requirements of the University of Glasgow for the degree of Master of Veterinary Medicine

by

Marta Hernandez Perez

DVM, MRCVS

School of Veterinary Medicine,

College of Medical, Veterinary and Life Sciences

February 2024

Abstract

Histopathology is a widely used method to assess the diagnosis of a variety of diseases and pathological conditions, and achieving a diagnosis is considered the ultimate aim in most cases, in order to prevent and/or treat possible diseases. Nevertheless, when it comes to research, the simple assessment of presence/absence of alteration is not considered precise enough, and a rigorous evaluation of affected tissues is needed, taking into account time-dependent factors and accurate determination of the severity of the changes in an unbiased way. Recent developments on image analysis software can reduce subjectivity and give the possibility to convert images into measurements which are in turn suitable for statistical analyses.

The purpose of this thesis was to explore the possibility of quantifying pathological changes using an unbiased method, using an image software (Image J). In that sense, a study was designed to test Image J on a previously used *ex vivo* organ culture (EVOC) system represented by canine and swine tracheal explants infected with canine influenza virus (CIV) and swine influenza virus (SIV), respectively.

While the role of the pathologist is still considered as an essential figure to develop the experiment and interpreting the results, Image J allowed the measurement of different parameters using immunohistochemistry (IHC) and H&E stains, allowing quantification of different pathological changes caused by influenza virus at different points of infection (from day 0 to day 4). These parameters were area of epithelium, apoptosis (cleaved caspase-3), innate immunity (Mx1), and regeneration (ki67). The results obtained in this study revealed changes consistent with epithelial loss, increased numbers of apoptotic cells, and regeneration in CIV- and SIV-infected tracheal explants, compared to non-infected ones.

Table of Contents

List of Figures

Acknowledgements

I would like to deeply thank my supervisor Prof Pablo Murcia for his constant support and for giving me the opportunity to join his research group at the CVR during my Research Master.

Special thanks go to Daniel Goldfarb who designed the macros used in my thesis and patiently trained me on using ImageJ.

Special thanks go to Julien Amat for his invaluable help with the statistical analysis.

Thanks to the VDS histopathology lab (Lynn Stevenson, Frazer Bell, Lynn Oxford, and Niamh Armstrong) for their amazing technical work and patient.

Thanks to the pathologists (my supervisor Dr Francesco Marchesi, Dr Angie Rupp, Dr Alex Gray, Dr Pamela Johnston, and Veronica Patton; as well as the previous ones, Dr Livia Thompson, Dr Caroline Millins, and Dr Cheryl Sangster) for their support and advice.

Thanks to the anatomic pathology residents, Kate Ings and Gail Chapman, for their friendship and unconditional moral support.

Thanks to the James Herriot Veterinary Small Grants Fund for their generous financial support to complete this thesis.

Thanks to the Clinical Pathology team and Prof Lubna Nasir, for allowing me to invade their offices during the COVID-19 pandemic.

Thanks to all my friends in Scotland, in the Canary Islands, and other parts of the world, for giving me the light that I need to keep going in the darkest moments.

Special thanks go to Dr Oscar Quesada from the ULPGC, for believing in me, even when I did not, and for showing me the wonderful world of Pathology.

To my father, my mother, and my sister. For always being by my side and encouraging me to follow my dreams, even when these bring me very far from home.

Author's Declaration

I, Marta Hernandez Perez, declare that, except where explicit reference is made to the contribution of others, that this dissertation is the result of my own work and has not been submitted for any other degree at the University of Glasgow or any other institution.

Marta Hernandez Perez

List of Abbreviations

CC3	Cleaved Caspase-3
CIV	Canine Influenza Virus
dip	days post-infection
EVOC	*ex vivo* Organ Culture (System)
HA	Hemagglutinin
hpi	hours post-infection
H&E	Haematoxylin and Eosin
IHC	Immunohistochemistry
IVs	Influenza viruses
NA	Neuraminidase
NP	Nucleoprotein
pfu	plaque forming unit
PB2	Polymerase Basic Protein 2
RIPK3	Receptor-Interacting Serine/Threonine-Protein Kinase 3
PRDC	Porcine Respiratory Disease Complex
PRRSV	Porcine Reproductive and Respiratory Syndrome Virus
SEM	Standard errors of the mean
SIV	Swine Influenza Virus
vRNPs	viral Ribonucleoprotein Complexes
VDS	Veterinary Diagnostic Services

1. Introduction

1.1. A brief overview on Influenza virus

Influenza viruses (IVs) are major respiratory pathogens for multiple animals and humans. IVs belong to the family *Orthomyxoviridae*, and are pleomorphic, spherical to filamentous viruses containing negative-sense single stranded RNA (Caswell & William, 2016). They are classified as *Alphainfluenzavirus* (Influenza A virus), *Betainfluenzavirus* (Influenza B virus), *Gammainfluenzavirus* (Influenza C virus), and *Deltainfluenzavirus* (Influenza D virus) genera, based on variation of the nucleocapsid proteins (ICTV, 2011).

Influenza viruses are named according to the World Health Organisation (WHO) classification published in 1980, and the features include the following: (1) antigenic subtype (e.g., A, B, C, D); (2) host origin (e.g., swine, equine, chicken), but for human-origin viruses, no host of origin designation is given; (3) the geographic origin of the isolate (e.g., Denver, Taiwan); (4) the unique laboratory or other reference identification number (e.g., 7, 15); (5) the year of isolation (e.g., 57, 2009); (6) the virus subtype, which are often included in parentheses at the end (e.g., H3N2, H1N1) (Centers for Disease Control and Prevention, 2023) (Vincent, et al., 2014).

Influenza A viruses (IAVs) are the most widespread and important members of the *Orthomyxoviridae* family, infecting different avian and mammalian species, including horses, dogs, pigs, seals, bats and humans (Centers for Disease Control and Prevention, 2023). Identification and classification of viral strains is based on the structure of the two surface glycoproteins, hemagglutinin (HA) and neuraminidase (NA), both embedded in the viral membrane, and at the time of writing, 18 different HA (H1-18) and 11 NA (NA1-11) have been identified (Centers for Disease Control and Prevention 2023) (Howley, et al., 2021).

IAVs change continuously due to their mutation rates and reassortment of gene segments, occasionally resulting in novel variants that cause pandemics and panzooties. There have been four human influenza pandemics since the beginning of the 20th Century. The devastating 1918 H1N1 pandemic resulted in an estimated 50-100 million deaths worldwide. The 1957 H2N2 and 1968 H3N2 pandemics were milder, but also caused 70000 and 34000 deaths, respectively, in the USA. The 2009 H1N1 pandemic, which began in the North American subcontinent, caught the world by surprise because preparedness efforts in that decade had focussed primarily

on H5N1 highly pathogenic avian influenza viruses, and the 2009 H1N1 pandemic virus was of swine origin. After each pandemic, the viruses became established in the human population and continued to evolve through antigenic drift over time, causing many epidemics and a substantial public health impact (Cox, et al., 2017).

1.2. Swine Influenza

Swine influenza is caused by swine influenza virus (SIV), an important global pathogen in the swine industry that causes acute respiratory disease in pigs. First documented cases in symptomatic animals were reported following the 1918 human cases of Spanish flu (Saunders-Hastings & Krewski, 2016). Currently, three main endemic subtypes have been identified in pigs (H1N1, H1N2, and H3N2) (Lyoo, et al., 2014), each subtype with different lineages and geographical circulation. In North America, the classical H1N1 SIV has been circulating after its first detection concomitant with the 1918 human pandemic. Following the introduction of the triple-reassortant H3N2 subtype in 1998 which contains genes of human, avian and swine origin, its spread and gene constellation drastically changed. The North American classical H1N1 lineage was first detected in European swine in 1976. In 1979 this lineage was replaced by the duck-derived avian-like H1N1 virus. H3N2 human IAVs and H1N2 human-avian reassortants are currently circulating in European pigs as well. In Asia besides the classical swine H1N1 and the European avian-like H1N1, an avian-like- H1N1 different from that circulating in Europe emerged in the 1990's representing another independent introduction of an avian virus into pigs, and European H3N2 and North American H3N2 have also been detected in this region (Vincent, et al., 2014).

The disease is characterised by high morbidity (may be exhibited at 100% in SIV-infected swine herd) and low mortality. SIV usually causes an abrupt outbreak of respiratory symptoms characterised by abdominal breathing and coughing, fever, nasal discharge, poor weight gain, and depression. Increased mortality is common due to secondary bacterial infections and co-infections with porcine respiratory disease complex (PRDC), especially *Haemophilus parasuis* and porcine reproductive and respiratory syndrome virus (PRRSV) co-infections (Richt, et al., 2003) (Lyoo, et al., 2014). Clinical signs start as early as 1 day post infection (dpi) in the

majority of experimental infections of swine with both swine and human isolates, and cease between 4 and 8 dpi.

Because the virus enters the lung through the airways, the most consistent macroscopic manifestation of influenza virus infection is cranioventral bronchopneumonia (Janke, 2014). The aerosol route of infection results in the movement of the virus through the conducting system (nasal passages and trachea) to the carina, and consequent spread into the short branches of the bronchial tree within the cranial and accessory lung lobes through gravity pull. Additionally, the anatomical anomaly of the tracheal bronchus in pigs may result in more lesions within the right cranial lung lobe (Detmer, 2017).

SIV primarily infects the epithelial cells lining the surface of the respiratory tract, from nasal mucosa and trachea to alveoli. Primary target cells for influenza viruses are cells of the respiratory epithelium (Fu Y, et al., 2019), leading to its hallmark histopathologic lesion of necrotising bronchitis and bronchiolitis (Janke, 2014).

The initial SIV lesions are seen as early as 24 hours post infection (hpi) and include vacuolar degeneration and necrosis of the epithelium with loss of the apical cilia. By 48 hpi, there is accumulation of sloughed necrotic epithelial cells and neutrophils within the airway lumen. By 72 hpi, the sloughing of epithelial cells is more prominent, and is admixed with mixed inflammatory cells. The remaining epithelial cells spread out to cover the basement membrane (attenuation), and the peribronchiolar lymphoid tissue expands, with increased numbers of lymphocytes and fewer macrophages (lymphoid hyperplasia).

Between 4 and 5 dpi, signs of recovery include epithelial hyperplasia, mitotic figures within the epithelial cells, and mild inflammation in the airways as the inflammation spreads outward, expanding the alveolar septa. By 7-10 dpi, there is variable interstitial pneumonia, perivascular and peribronchiolar lymphoid proliferation, and normal to hyperplastic bronchial epithelia. Between 11 and 21 dpi, there is fully recovery of the damaged respiratory tissues at the microscopic level. During recovery, bronchiolar polyps and bronchiolitis obliterans may occur (Detmer, 2017).

1.3. Canine influenza

Epidemics of influenza viruses in dogs are relatively recent developments. Canine influenza virus (CIV) was first recognized in 2004 when an outbreak of severe respiratory distress was seen in greyhounds in Florida, USA, identified as subtype H3N8 (Crawford, et al., 2005). In 2007, a second CIV, the H3N2 influenza A virus, caused a disease outbreak in pet and farmed dogs in South Korea (Lee, et al., 2009). Each of the CIV epidemics ultimately derived from a single cross-species transfer event, with the H3N8 subtype transferring from horses, while the H3N2 subtype arising from an avian reservoir.

H3N8 CIV, the one that the current study is focused on, had spread to at least 11 states in the USA by 2004, mostly by transport of infected racing greyhounds, and had also already spread also to pet dogs and animals in shelters and kennels in the USA. Since about 2007, CIV has been primarily maintained in a small number of large shelters in big metropolitan areas, and it is suggested that these viruses are frequently transferred to other populations of dogs, resulting in outbreaks (Parrish & Dubovi, 2017).

Both H3N8 and H3N2 CIV infections in dogs most often cause a mild or subclinical upper respiratory tract disease, often including coughing, fever, and anorexia, although severe illness is sometimes associated. The incubation period lasts 2-3 days, and viral shedding has been observed from day 2-7 after exposure to the virus, with symptoms between days 3-14 post infection.

Mild disease caused by H3N8 infection in dogs is associated with typically moist cough, although it can also be dry. Symptoms may last for 7-10 days, and animals usually recover uneventfully. Pneumonia, including haemorrhagic pneumonia, can develop. Symptoms might be exacerbated by co-infections with other pathogens, and in one study co-infection with *Streptococcus equi* subspecies *zooepidemicus* resulted in much more severe disease and lung involvement than did with either pathogen alone (Larson, et al., 2011).

The H3N2 virus generally causes a mild upper respiratory tract disease, although the severity of disease may be greater than that caused by H3N8 CIV, with severe interstitial pneumonia, high fever and bronchioalveolitis (Kang, et al., 2013). Most viral replication has been identified in the respiratory tract, although some virus has also been detected in other organs, including liver, spleen, kidney, brain, and duodenum (Parrish & Dubovi, 2017) (Zeng, et al., 2013).

Infection of the lungs may occur in both H3N8 and H3N2 CIVs, and that might be also associated with death, commonly linked to mixed infections by other viruses or bacteria, or with other health issues for the dogs (Parrish & Voorhees, 2019).

Histologically, CIV infection causes tracheobronchial epithelial cell necrosis, hyperplasia, and inflammatory infiltration. Less frequent cases with involvement of distal airways show bronchiolar erosion or hyperplasia, and bronchi-alveolar inflammatory infiltrates (Caswell & William, 2016).

1.4. The use of *ex vivo* organ cultures as complementary models of influenza infection

Over the years, *ex vivo* organ cultures deriving from different poultry species, humans, pigs, dogs and other animal species have been developed. Such systems reproduce, to a great extent, the physiological conditions and the cellular complexity of the respiratory mucosa of the host in a highly controlled setting. *Ex vivo* organ culture (EVOC) of tracheal explants with an air-liquid interface system have been used in the study of both human and animal respiratory pathogens (Nunes, et al., 2010) as they represent to a great extent the natural site of infection of respiratory viruses. Consequently, they have been broadly used to study the infection biology of many viruses including IAVs, severe acute respiratory syndrome coronavirus 2 (SARS-CoV-2), and respiratory syncytial virus (RSV) (Hui, et al., 2020).

EVOC systems to study influenza were first reported in 1974, showing that respiratory tissue cultures were viable for at least 48 hours without major changes, and indicating their suitability for studying viral replication (Schmidt, et al., 1974). Regarding IAVs, back-to-back infections of pigs and ALI-cultures derived from pigs with different isolates of pdmH1N1 showed that the infection phenotype of ALI-cultures can be used to predict *in vivo* virulence (Fu, et al., 2019). Importantly, as explants lack any component of adaptive immunity, they allow to evaluate cellular responses to infection, such as the IFN response, at the natural site of infection, excluding systemic responses.

By infecting explants with a known dose of virus and collecting samples at different time points, EVOC systems allow a qualitative and/or quantitative analysis of many aspects related

to infection and host response such as viral growth, identification of target cells, mechanisms of cellular response to infection (apoptosis, regeneration), and innate immune host responses. Furthermore, tissue collected from a single animal can be used in numerous replicas, reducing experimental variability and the number of animals used, in accordance with the 3R's principles (reduction, replacement and refinement) in animal experimentation (Russell & Burch, 1959).

The *ex vivo* technique, however, has some limitations in type of data it can provide. When testing the replication potential of avian, human and swine influenza viruses in swine explants, Van Poucke and colleagues confirmed that the observed data had maximal similarity to the *in vivo* situation in previous studies (Van Poucke, et al., 2010). On the other hand, Chambers and colleagues, in a study aiming to evaluate the replication of avian influenza viruses in equine tracheal explants and ponies, found incongruent results, in that none of the viruses that replicated in tracheal explants was able to infect ponies *in vivo* (Chambers, et al., 2013). This provides evidence that organ explants are useful tools to obtain tissue-specific data on virus infectivity but that the physiological and immunological barriers in the living host might be far more difficult to overcome. Additionally, the absence of a blood supply constitutes a weakness of the interface EVOC system as recruitment of cells of the immune system to the infection site is prevented.

1.5. Quantification of disease severity

Histopathological examination is a powerful tool to investigate a disease condition by directly observing morphological changes in different tissues in both clinical and nonclinical settings. However, these evaluations are qualitative or semiquantitative, and several factors, including technical aspects of tissue processing and inter-observer variability, can introduce bias that impacts the consistency and reproducibility of the results across laboratories/institutions and across different experiments within the same laboratory.

Evaluation by multiple experienced pathologists can increase objectivity and improve the reliability in a diagnostic setting. However, in clinical research studies and with experimental models, the pathologist is called not only to assess the presence/absence of morphological alterations in the selected tissues, but also to identify and substantiate differences amongst

experimental groups. Moreover, if quantitative analysis of pathological evaluations is automated, it can improve efficacy, save labour, and speed-up evaluation (Horai, et al., 2019).

The use of digital pathology has rapidly increased in recent years, enabling the use of image processing software analysis to quantify morphological changes of pathological tissues. Examples of image software that have been used to quantify different histopathological diseases include Image J, HALO, Genie, and others (Daunoravicius, et al., 2014) (Horai, et al., 2019).

Although the role of the pathologist is irreplaceable for setting up the software and verify its progress, the computer-based image analysis can overcome the intrinsic biases of semi-quantitative scoring, providing a more objective, precise, and accurate assessment. Another powerful advantage is that it is also able to provide quantified measurements suitable to more robust further statistical analysis (Horai, et al., 2019).

The aim of this work was to quantify pathological changes and specific endpoints (including cellular localisation of viral nucleoprotein, cellular innate anti-viral response, apoptosis and cellular replication) induced by H3N8 CIV and H3N2 SIV in an *ex vivo* organ culture (EVOC) system consisting of canine and swine tracheal explants, respectively. To this end, histological and immunohistochemical analyses of archived material were performed (Gonzalez, et al., 2014) (Patrono, et al., 2015) and quantified pathological endpoints using digital pathology approaches.

2. Materials and Methods

2.1. Explant preparation

This study was performed on formalin fixed paraffin embedded block tissues developed and prepared in two previous studies. Swine explants and paraffin blocks were prepared by Livia Patrono for her doctoral degree (Patrono, et al., 2015), whereas canine explants were produced by Gaelle Gonzalez (Gonzalez, et al., 2014). Both canine and swine tracheal explants were prepared as per description in Nunes (Nunes, et al., 2010) and Gonzalez (Gonzalez, et al., 2014).

Swine tracheas were collected from commercial hybrid female piglets from a high health status farm, serologically negative against influenza virus. Dog tracheas were collected from healthy beagles from Charles River Laboratories used as negative controls in other, unrelated studies. Upon euthanasia, the tissues were aseptically collected and transported to the laboratory in a prewarmed medium for explant preparation (Figure 1).

After different washing steps, the connective tissue surrounding the cartilage was removed and tracheas were opened lengthways and cut into squares of approximately 0.5 x 0.5 cm.

All explants were prepared according to the air-liquid interface culture method, using a technique described by Nunes and colleagues, which consists of mimicking the physiological condition of respiratory tract tissues that receive nutrients from the blood and are exposed to air (Nunes *et al.*, 2010).

After 24h of culture swine explants were infected with 200 plaque forming units (pfu) of H3N2 SIV (A/swine/Italy/8088/23006), and canine explants were infected with H3N8 CIV (A/canine/New York/51864/2008). Samples were collected at different time points post infection (0, 1, 2, 3, 4 days post infection). Afterwards, infected and control explants were placed in 10% formalin and routinely processed for histopathological assessment.

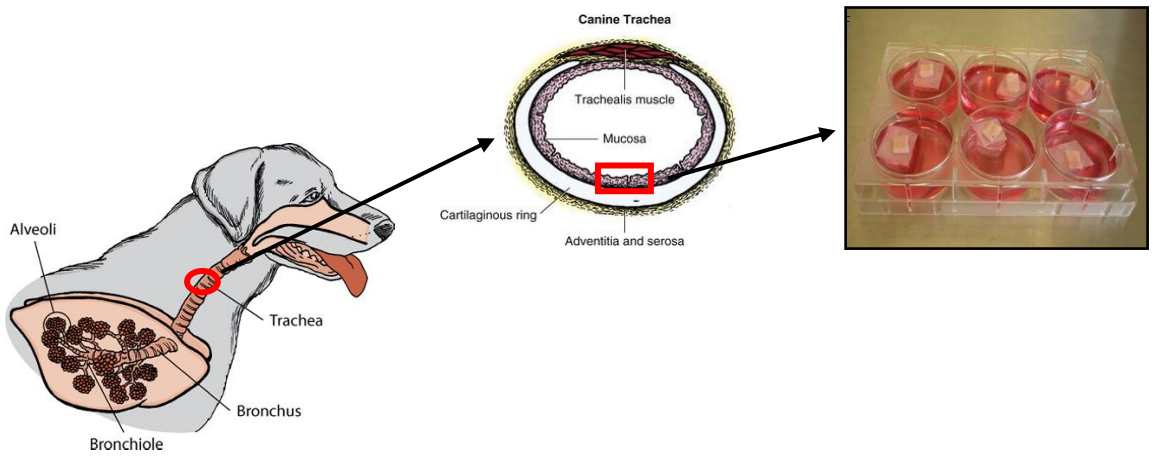

Figure 1. Canine tracheal explant preparation.
The trachea is removed immediately upon euthanasia. Small (approximately 0.5 x 0.5 cm) fragments of mucosa are removed from the underlying cartilage and placed in an air-liquid interface plate.

2.2. Haematoxylin & Eosin and Immunohistochemistry

Explants were fixed in 10% buffered formalin and paraffin embedded by Patrono (Patrono, et al., 2015) and Gonzalez (Gonzalez, et al., 2014). The current study started on cutting the paraffin embedded blocks. Multiple 2 µm serial sections were obtained from each explant (control, and CIV and SIV infected explants) and stained with Haematoxylin and Eosin (H&E), and multiple 3 µm serial sections immunostained using various antibodies, including rabbit polyclonal anti Influenza NP (European Veterinary Labs), rabbit polyclonal anti-Cleaved Caspase 3 (R&D Systems), mouse monoclonal anti-MX1 (provided by Georg Kochs), and mouse monoclonal anti-ki67 (Dako).

The slides were pressure-cooked (Menarini Diagnostic) in pH 6.0 sodium citrate buffered solution for the remaining primary antibodies (i.e. CC3, ki67 and MX1). Endogenous peroxidase was blocked with 3% hydrogen peroxide + PBS.

After blocking, slides were incubated for 30 min at room temperature with the primary antibodies at the following dilutions: anti-NP 1:400, anti-Cleaved Caspase 3 1:400, anti-MX1 1:500 for swine blocks and 1:1000 for canine blocks, and anti-ki67 1:200 for swine explants.

Several attempts with different solutions (1:200 and 1:500) were tried for anti-ki67 in canine explants; however, the ki67 signal appeared very weak, and some clearly identifiable mitotic figures (expected to be ki67 positive) were lacking any ki67 signal.

Mouse EnVision/HRP (Dako, Agilent) or Rabbit EnVision/HRP (Dako, Agilent) were used as secondary antibodies.

Liquid DAB (3.3'-Diaminobenzidine) + Substrate Chromogen System (Dako, Agilent) was used as the visualisation step.

Sections were counterstained with Mayer's haematoxylin, dehydrated in ascending alcohol cleared in histoclear, and coverslipped.

Images were taken at 40x magnification with an Olympus CX31 microscope. Three images per section per timepoint were acquired and repeated for each staining. Additionally, every staining was measured on three sections.

2.3. Histological analysis in H&E samples

A first manual assessment of the H&E samples (control and CIV/SIV infected explants) was carried out using an OlympusCX31 microscope to evaluate the presence or absence of histopathological changes (such as loss of cilia and goblet cells, attenuation of the epithelium, presence of apoptotic cells, or presence of mitotic figures) in CIV/SIV samples compared to the controls. This is a crucial step in order to decide which histological changes wanted to be evaluated and quantified, and which IHC stains would be needed to use for this purpose.

2.4. Image analysis

2.4.1. ImageJ

Image analysis was carried out on ImageJ, which is a free image analysis software developed by the National Institutes of Health (NIH) and the Laboratory for Optical and Computational

Instrumentation (LOCI, University of Wisconsin) for low-level processing of digital images (Collins, 2007) (Schneider, et al., 2012). It is used in a wide range of science and engineering fields such as medical imaging, microscopy, the material sciences, and biological light microscopy.

The program is written in Java, and compatible with majority of current operating systems (including Linux, Mac OS X and Windows). ImageJ supports a wide number of standard image file formats (including TIFF, PNG, GIF, JPEG, BMP, PNG, FITS, DICOM, and ASCIL), as well as raw formats (Schneider, et al., 2012).

The software incorporates a number of several useful tools for image processing. These include histogram manipulations and standard image filters (mean, median, etc.) and other user-written plugins for more sophisticated filtering.

The internal macro programming language of ImageJ is a simple text-based scripting language that can be used just to automate multiple processing and analysis steps, but also can be designed to perform very sophisticated routines. The initial macro can be further developed using macro programming language and can be modified to suit specific needs.

Measurements are created in pixel numbers, and histograms and profile plots are generated. Thus, the intensity of specific staining such as those produced by immunohistochemistry and immunofluorescence can be evaluated in a quantitative way (Collins, 2007).

2.4.2. Quantitative score

All the histological images analysed were collected using cellD* Software (Olympus). For each antibody and for each timepoint, 3 photomicrographs at 400x magnification were taken from the central portion of the sections from control and CIV/SIV infected explants to avoid crush artefacts generated by sampling and mostly evident at the edges of the slide samples. Specific macros for quantification of the IHC (NP, CC3, MX1, and ki 67) within the respiratory epithelium were developed by Dr Daniel Goldfarb using ImageJ software.

Epithelium areas were manually selected, to exclusively restrict the analysis to the epithelium compartment, and length and area of the epithelium was measured. Images were colour deconvoluted (Schneider, et al., 2012) to separate brown (DAB) to blue (nuclei) channels, and

default automatic thresholding was used to identify areas of positive signal. The picture generated in the DAB channel was then converted in a binary picture (black and white), and the amount of positive signal was measured in terms of number of stained pixels. The number of pixels obtained for each marker was then normalised by the length of the explants (previously manually selected and measured).

A flowchart with the quantification steps is shown in Figure 2.

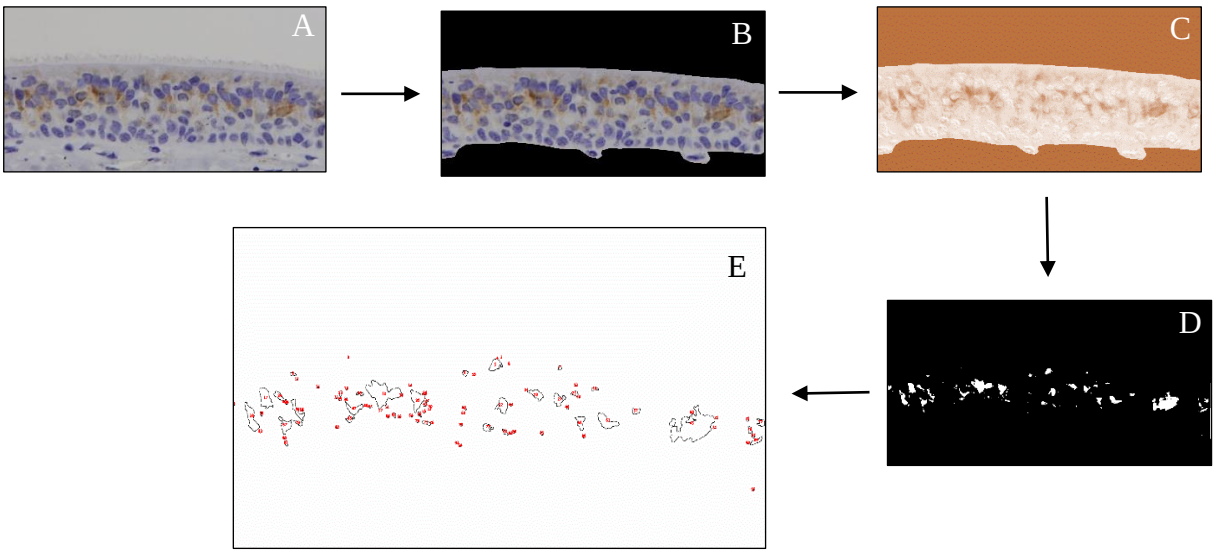

Figure 2. IHC quantification using ImageJ.

The most salient steps of IHC signal quantification in the respiratory epithelium are summarised as follows. Representative pictures of stained explants were collected at 400x (A). The respiratory epithelium was manually selected and cropped (B). Following colour devolution, the positive signal was extracted in the DAB channel (C). The obtained picture is then converted to a binary picture (D), and the number of pixels is quantified (E).

2.5. Statistical analysis

Results were reported as mean ± standard errors of the mean (SEM) of multiple independent measurements. The number of measurements varied depending on the parameter and it is specified for each parameter in the results section. A minimum of 246 images (50% non-infected (control) and 50% infected explants) were analysed for each parameter and each

animal species (swine and canine). Data were collected and compiled into excel spreadsheets before analysis. Statistical analyses were carried out using R studio v3.5.1 software. Multivariable logistic models were used to investigate associations between normalised signal area (NP, Mx1, CC3) or epithelium area and infectious status (infected/non-infected) and time post-infection, in either dogs or pigs independently. Multivariate logistic models were built using the "glm()" function (family = "gaussian"), and used infectious status and time as predictors, while stained area was used as the response variable. Models can be summarised by the following equation:

$$Stained\ Area\ (continuous) \sim Time\ (integer) + Infectious\ status\ (binary)$$

Significance levels are shown as *** $p<0.001$, ** $p<0.01$, and * $p<0.05$.

Models' goodness of fit was individually assessed using the DHARMa package version 0.4.1. If goodness of fit was not satisfied, model analysis was dropped and non-parametric test, such as Wilcoxon Man Whitney, was alternatively used for each time point, staining and species individually. This methodology was applied for Mx1 expression, as the multivariate logistic model goodness of fit was poor.

3. Results

3.1. Histopathological changes in swine and canine tracheal explants experimentally infected with Influenza Virus

In vivo studies have provided valuable information on clinical course, viral pathogenesis, innate and acquired immune responses, vaccine efficacy and antiviral treatment. However, such studies are greatly affected by animal welfare considerations and logistical constraints.

To overcome such constrains, *ex vivo* organ cultures (EVOC) of tracheal explants have been successfully developed.

EVOC systems reproduce and retain all the histological features of a normal respiratory mucosa, including a pseudostratified ciliated columnar epithelium and scattered goblet cells (Figure 3). The three-dimensional structure and cell diversity of the respiratory mucosa is preserved together with important physiological features like normal expression levels of cell receptors, effective mucus production and ciliary activity.

The samples used in this research project consisted of archived formalin-fixed paraffin-embedded tracheal explants from three dogs and three pigs prepared in two previous studies as detailed in Material & Methods (Gonzalez, et al., 2014) (Patrono, et al., 2015).

Firstly, the H&E stained sections from the mock-infected and virus-infected (either with CIV or SIV) explants were qualitatively assessed using an Olympus CX31 microscope, with the purpose to identify histopathological changes in the mucosal epithelium caused by SIV in swine tracheas and CIV in canine tracheas.

Virus-induced changes consistently observed in both species included loss of cilia and cells, epithelial degeneration and regeneration.

Complete or partial loss of cilia was evident in samples infected with either CIV or SIV (Figure 3). However, some variability on cilia preservation was noted in the mock explants, and therefore, loss of cilia was not included as an endpoint suitable for reliable quantitative assessment as part of this thesis.

Cellular loss was represented by loss of the outer epithelial cellular layer and reduction in the number of Goblet cells, leading to a reduction of the epithelial area/thickness (Figure 3).

Cellular degeneration was represented by multifocal flattening of epithelial cells, occasional epithelial vacuolation, karyorrhexis, and increased apoptosis. Sloughed, karyorrhectic epithelial cells and cellular debris over the tracheal epithelial surface were also observed in infected explants. Apoptotic cells were recognised as shrunken cells with hyper-eosinophilic cytoplasm, in concurrence with pyknotic or fragmented nuclei.

Low numbers of mitotic figures only restricted to the basal layer are expected in a normal tracheal epithelium; nevertheless, a slightly increased number of mitotic figures scattered throughout the full thickness epithelium was detected in the infected explants and interpreted as a manifestation of regeneration.

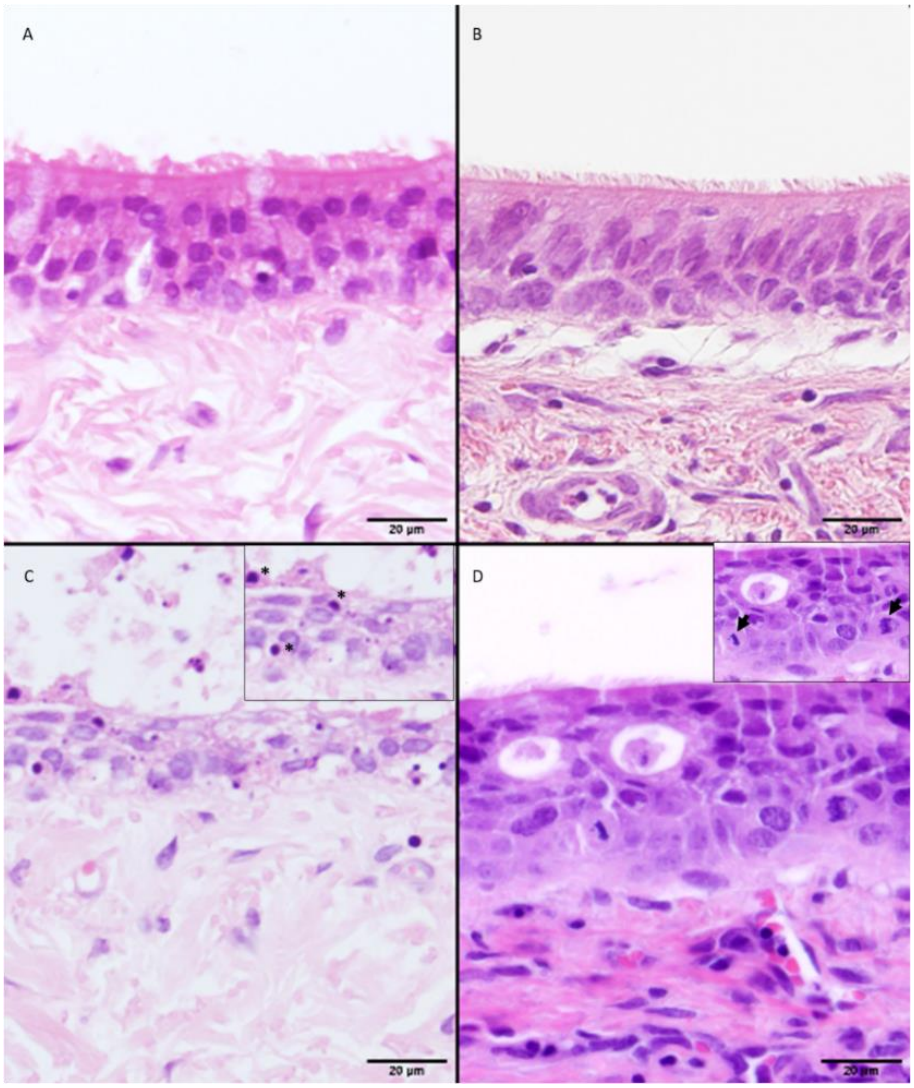

Figure 3. Histopathological features of CIV and SIV infection.

Representative microphotographs illustrating the major histopathological changes observed in canine and swine tracheal explants infected with CIV or SIV, respectively (H&E). Control (non-infected) explants of canine (A) and swine (B) explants exhibit a pseudostratified ciliated columnar epithelium with scattered goblet cells, whereas CIV-infected CIV (C) and SIV-infected (D) explants exhibit diffuse loss of cilia and outer layers of the epithelium, and attenuation of the epithelium. CIV explants also show sloughed degenerate epithelial cells within the tracheal lumen. Inset, C: scattered apoptotic cells (asterisk) are noted throughout the tracheal epithelium in CIV infected explant. Inset, D: Occasional mitotic figures (arrows) are seen as sign of regeneration.

3.2. Immunohistochemical investigation of the markers of infection and cellular response (NP, CC3, Mx1 & ki67)

3.2.1. Nucleoprotein (NP)

To establish a correlation between the presence of the virus in the infected samples and the histopathological changes previously described, viral nucleoprotein (NP) immunohistochemistry was performed in all the samples (CIV- or SIV-infected and control tracheal explants). NP displayed an irregularly dotted signal, ranging from moderately to highly intense brown staining in the nuclei, and to a lesser extent, in the cytoplasm, of well-preserved and degenerate epithelial cells, commonly including positive sloughed degenerate epithelial cells within the tracheal lumen (Figure 4).

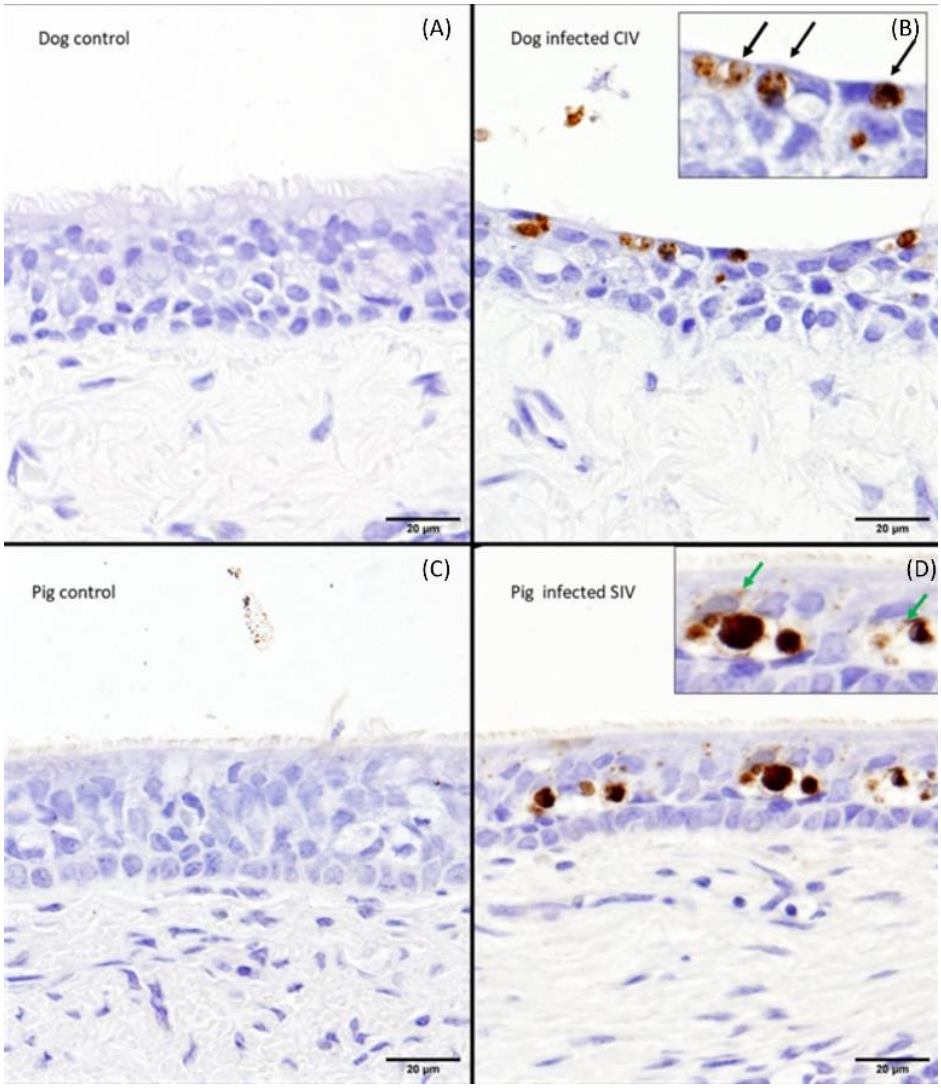

Figure 4. Representative microphotographs of NP localisation. NP staining was characterised by an irregularly dotted brown signal in the nuclei (B - black arrows), and occasionally intracytoplasmic (D - green arrows), within the mucosal epithelium of CIV/SIV infected explants.

3.2.2. Cleaved caspase 3 (CC3)

After observing cellular death morphologically consistent with apoptosis in the first assessment of the H&E sections, confirmation and quantification of this wanted to be assessed. For this purpose, immunohistochemistry for cleaved caspase 3 (CC3) was performed.

Caspases are crucial mediators of programmed cell death (apoptosis), and among them caspase-3 is a frequently activated death protease, catalysing the specific cleavage of many key cellular proteins. This caspase is responsible for the majority of proteolysis during the execution phase of apoptosis, and detection of cleaved caspase-3 is therefore considered a reliable marker for cells that are dying or have died by apoptosis (Gown & Willingham, 2002).

CC3 demonstrated a light to moderately strong brown pattern in the nucleus and/or cytoplasm of shrunken epithelial cells with condensed nucleus and in cellular fragments of dead cells (Figure 5).

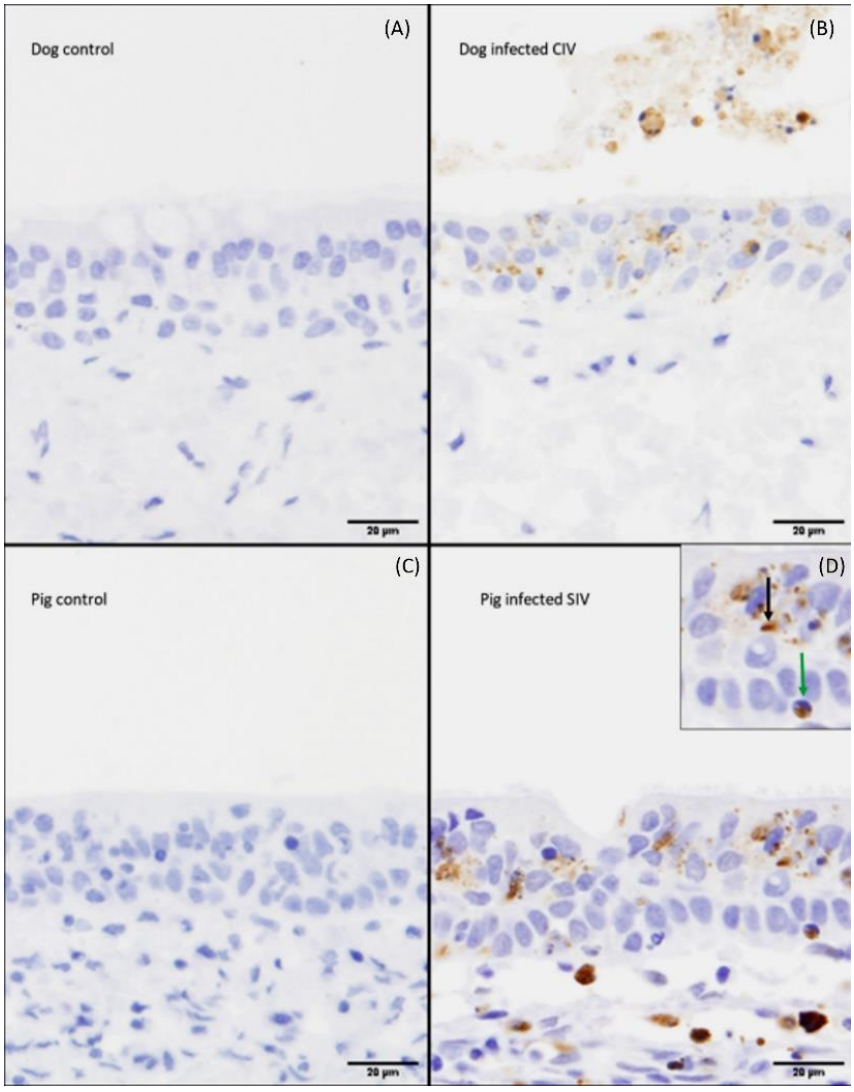

Figure 5. Representative microphotographs of CC3 expression. CC3 staining was characterised by a nuclear/cytoplasmic pattern of staining in commonly shrunken cells with condense nucleus (inset D - green arrow), as well as in disrupted/fragmented cells (inset D - black arrow).

3.2.3. Interferon-induced GTP-binding protein Mx1

Interferon-mediated host factors myxovirus (Mx) proteins (also known as Mx1 and Mx2 proteins) are considered to be self-autonomous host restriction factors of the innate immune system against many DNA and RNA viruses (including influenza A viruses) (Fatima, et al., 2019). Their precise mechanism of action is still under investigation; however, studies on MxA gene (the human orthologue of the murine Mx1 gene) have

suggested that its oligomerisation forms a ring-like structure that binds to NP and prevents nuclear import of viral ribonucleoprotein complexes (vRNPs), aborting viral replication (Turan, et al. 2004).

Immunohistochemistry for Mx1 was performed on the sections from control and CIV- or SIV-infected explants to identify levels of total Mx1 protein and quantify changes of Mx protein expression as a proxy of innate immune activation (Fatima, et al., 2019).

Positive stain was restricted to the cytoplasm of epithelial cells, with expression varying from faint to very intense (Figure 6). Mx1 expression, to lower levels, was also expected in control explants.

Adaptive immunity could not be investigated in canine and swine explants because of the intrinsic *ex vivo* nature of the EVOC system.

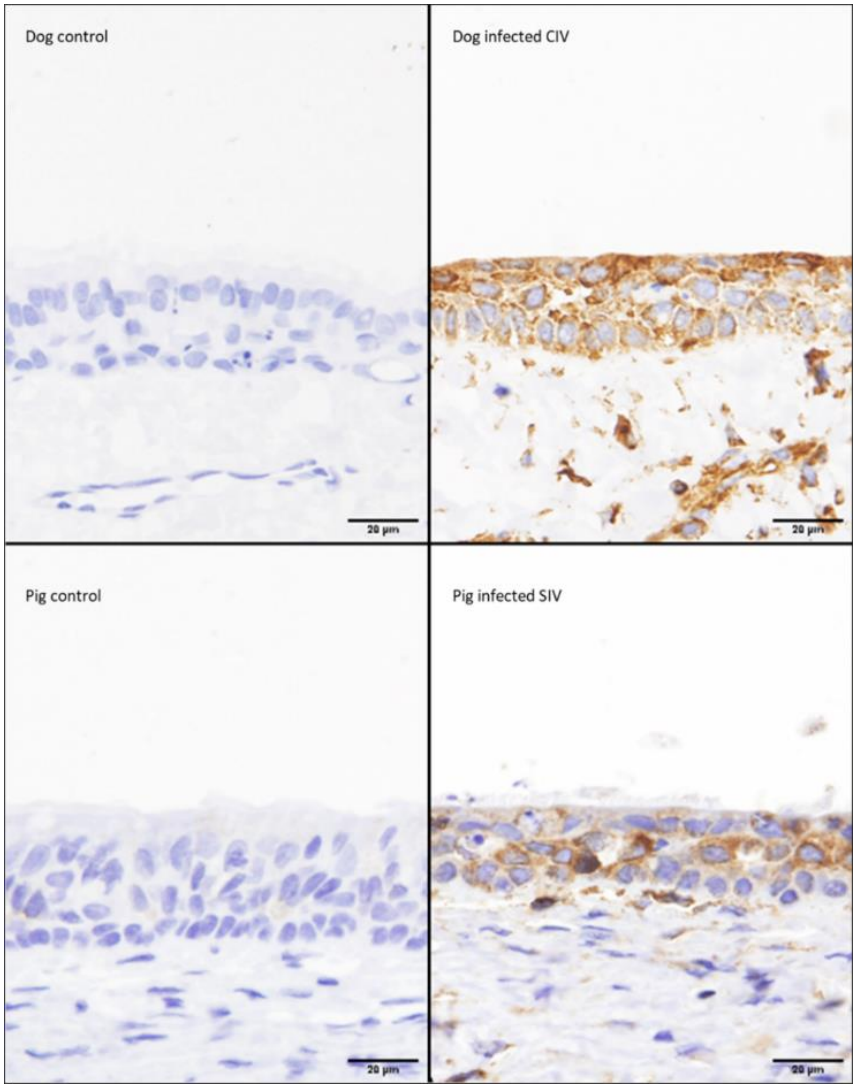

Figure 6. Representative microphotographs of Mx1 expression. Mx1 positive signal is strictly cytoplasmic.

3.2.4. Ki67

Hyperplasia of the respiratory epithelium is described in the literature as a common finding in animals infected with influenza virus, indicating regeneration, represented by an increased number of mitotic figures along the full thickness epithelium (Caswell and Williams, 2016). As stated previously, preliminary qualitative examination of the samples revealed an increase in the number of mitotic figures in tracheal epithelium infected with CIV and SIV, particularly at day 3 post infection.

Ki67 is a very well-known proliferation marker present in all the active phases of the cell cycle (G1, S, G2, and mitosis), and absent from resting cells (G0) (Maglennon, et al., 2008). It accounts for an expression strictly restricted to the nucleus (Vascellari, et al., 2012).

Quantification of ki67 expression was included as an endpoint in this project, to assess regenerative changes caused by CIV and SIV infection in tracheal explants.

3.2.4.1. Ki67 expression in swine explants

In swine explants, ki67 expression was exclusively present in the nuclei of epithelial cells, with a staining pattern ranging from weakly stippled to strong and homogeneous. Ki67 expression in scattered cells in the basal layer was expected, as a physiologic process, in the control explants; conversely, positively stained nuclei were scattered throughout the full-thickness epithelium in the infected samples (Figure 7).

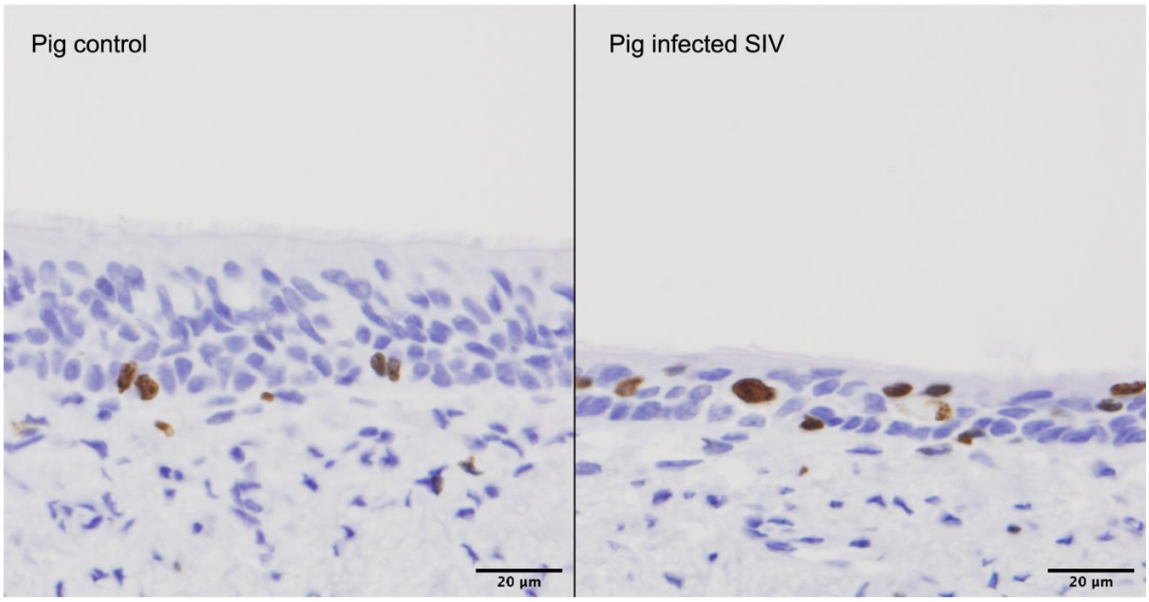

Figure 7. Representative microphotographs of ki67 staining in swine explants. Ki67 expression was characterised by weak to strong nuclear staining. Positive nuclei were restricted to few scattered cells in the basal layer in control explants, whereas ki67 positive nuclei were scattered throughout the full epithelial thickness in SIV infected samples.

3.2.4.2. Limitations of ki67 expression in canine explants

While staining with the anti-ki67 antibody in swine tracheal explants showed a clear nuclear positive signal in proliferating cells, the results in canine explants were inconsistent. Despite attempts with different antibody concentrations (1:200 and 1:500) the ki67 signal appeared very weak, and some clearly identifiable mitotic figures (expected to be ki67 positive) were lacking any ki67 signal (Figure 8).

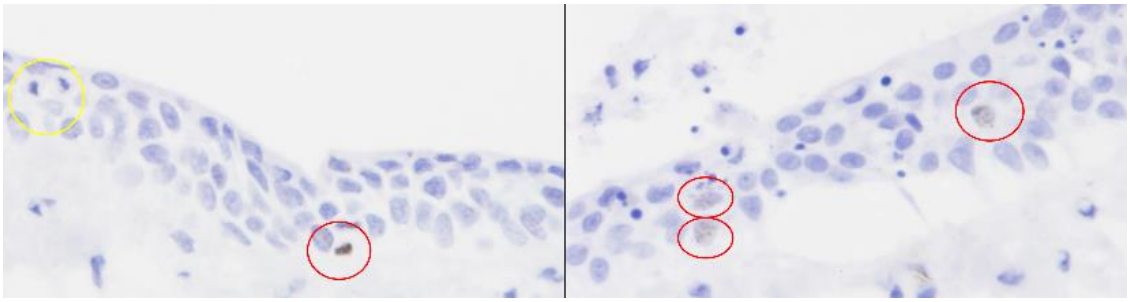

Figure 8. Representative microphotographs of ki67 staining in canine explants. Positive ki67 cells (red circles) show faint granular expression. An evident mitotic figure (yellow circle) lacks ki67 signal.

3.3. Quantification of histopathological and immunohistochemical changes

To adopt a robust and unbiased method to quantify pathological changes in the trachea of dogs and pigs infected with CIV or SIV, respectively, Image J was used to quantify different parameters in the H&E and IHC stained sections.

For all the H&E-stained samples and the immunohistochemical markers, 3 microphotographs per section were captured at high power magnification (400x). Every sample had 2 to 3 sections, and therefore a total of 6 to 9 microphotographs per timepoint (0 to 4 dpi) were captured for both control and infected explants.

3.3.1. Quantification of the area of the epithelium

The area of the epithelium was obtained from 472 images (240 from canine explants and 232 from swine explants) taken from H&E, NP, CC3, and Mx1 stained sections. The number of total pixels was normalised by the length of the epithelium for every image (magnification field 400x).

3.3.1.1. Canine explants

In the canine explants, the area of epithelium was lower in the infected samples compared with controls at all time points. The decrease was particularly prominent at day 2 post-infection, and remained relatively stable until day 4.

Statistically significant ($p<0.01$) differences were appreciated between control and CIV infected explants at 2 dpi, and highly significant at 3 and 4 dpi (multivariate GLM test) (Figure 9).

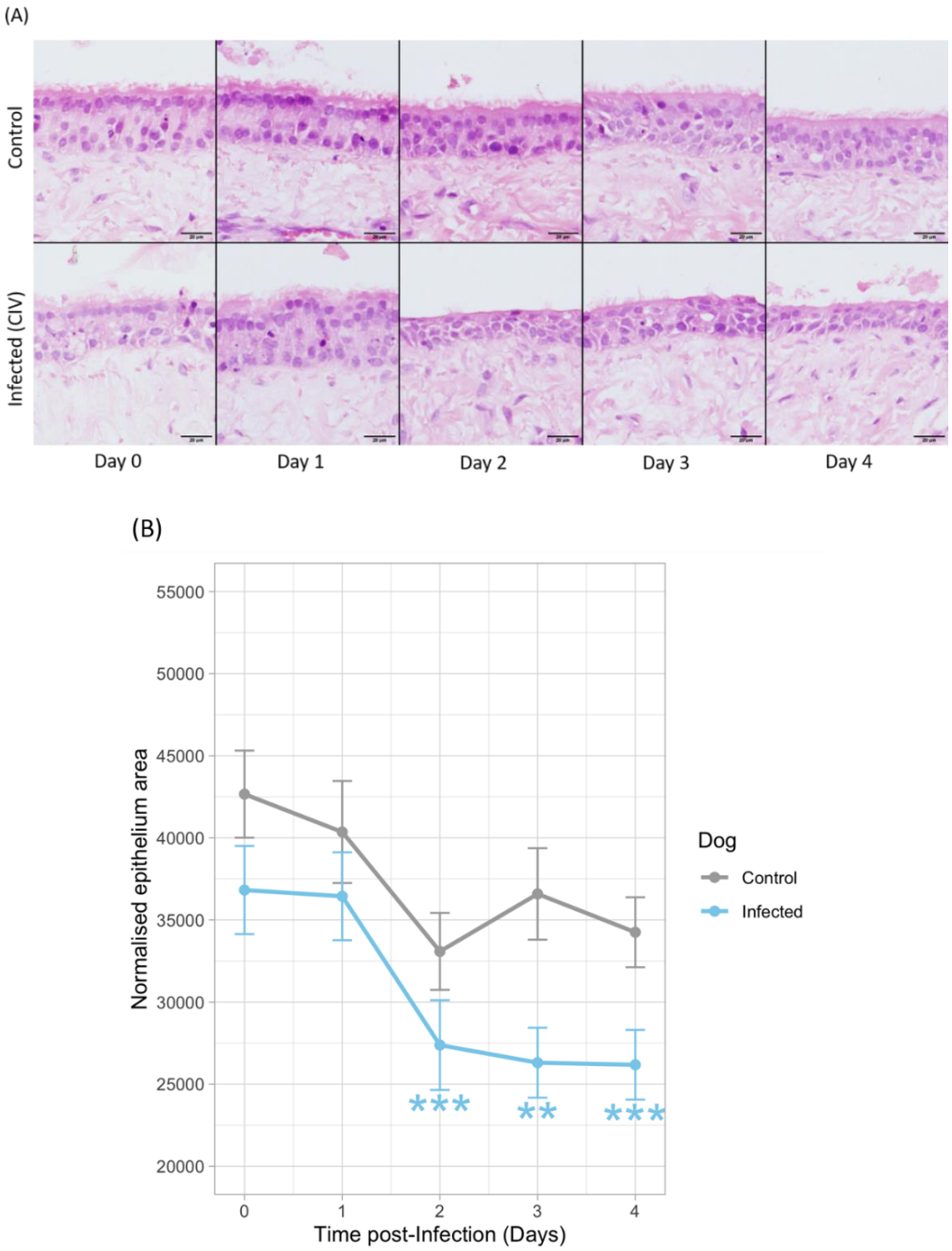

Figure 9. Representative microphotographs (A) and quantification of epithelial area (B) in canine tracheal explants. Control and CIV infected explants, representative images at 0, 1, 2, 3, and 4 dpi, H&E (A). Quantification of the area of the epithelium (normalised), measured in pixels, in canine control and CIV infected explants. Point estimates are means and bars are standard errors of the mean. Significance levels are shown as *** $p<0.001$, ** $p<0.01$, and * $p<0.05$ (B).

3.3.1.2. Swine explants

SIV-infected explants showed a trend towards a decrease in epithelial area compared with control at 3 and 4 dpi; however, these differences were not statistically significant ($p \geq 0.5$) (multivariate GLM test) (Figure 10).

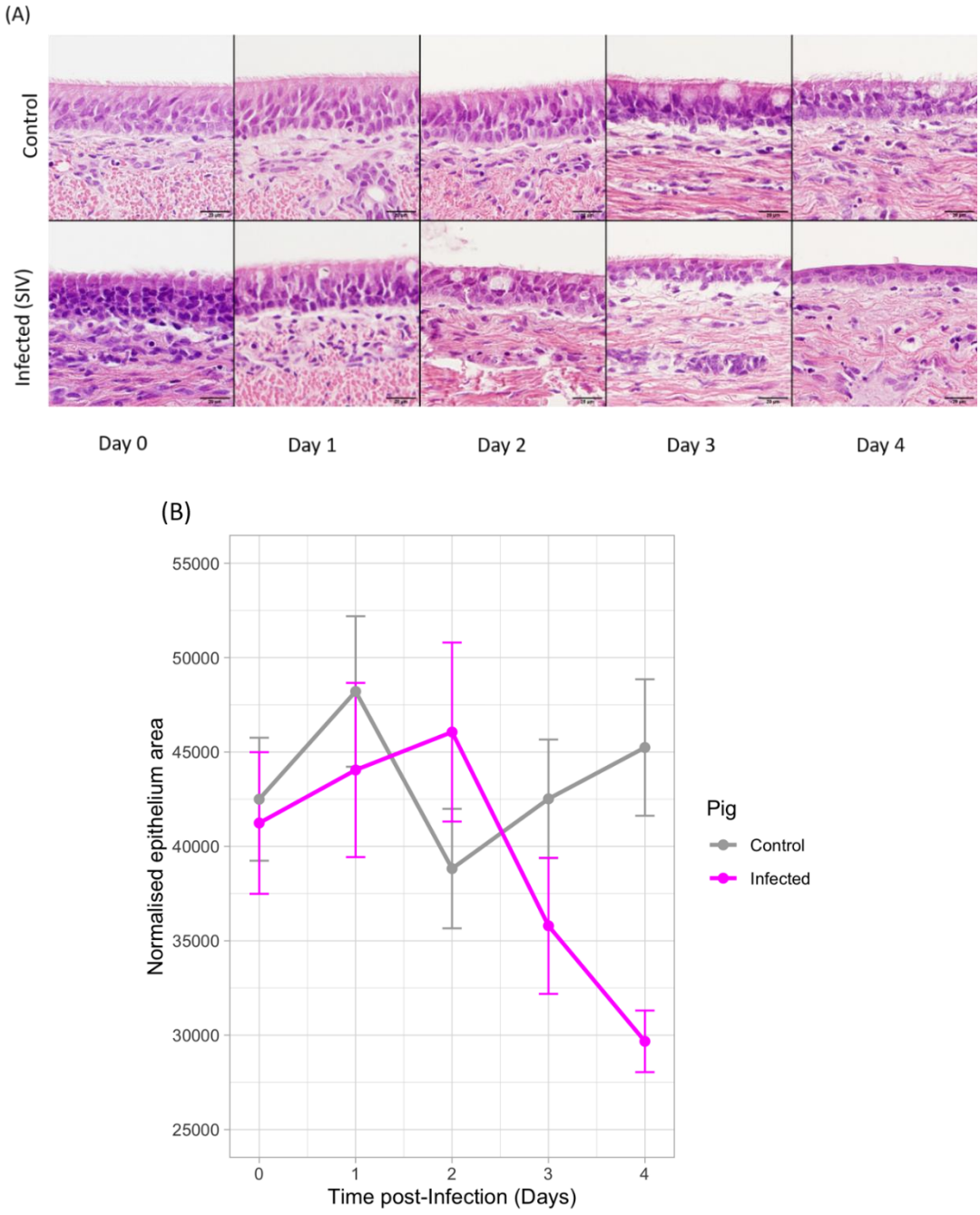

Figure 10. Representative microphotographs (A) and quantification of epithelial area (B) in swine tracheal explants. Control and SIV infected explants, representative images at 0, 1, 2, 3, and 4 dpi, H&E (A). Quantification of the area of the epithelium (normalised), measured in pixels, in swine control and SIV infected explants. Point estimates are means and bars are standard errors of the mean. Significance levels are shown as *** $p<0.001$, ** $p<0.01$, and * $p<0.05$ (B).

3.3.2. Quantification of NP expression

NP expression was quantified in a total of 252 images from the canine explants and 270 images from swine explants. The number of total pixels obtained for NP signal was normalised by the area of the epithelium. In both species, NP demonstrated its presence in explants infected with either CIV or SIV from day 1 to day 4 post-infection. Scant signal was noted in control explants; however, the percentage of NP positive pixels was close to 0%. This finding was interpreted as non-specific stain.

3.3.2.1. Canine explants

Canine explants exhibited the peak of NP signal at 2 dpi to progressively decrease until 4 dpi.

Statistically, highly significant ($p<0.001$) differences were seen between control and CIV infected explants at 1, 2 and 3 dpi, and to a lesser extent ($p \leq 0.05$) at 4 dpi (multivariate GLM test) (Figure 11).

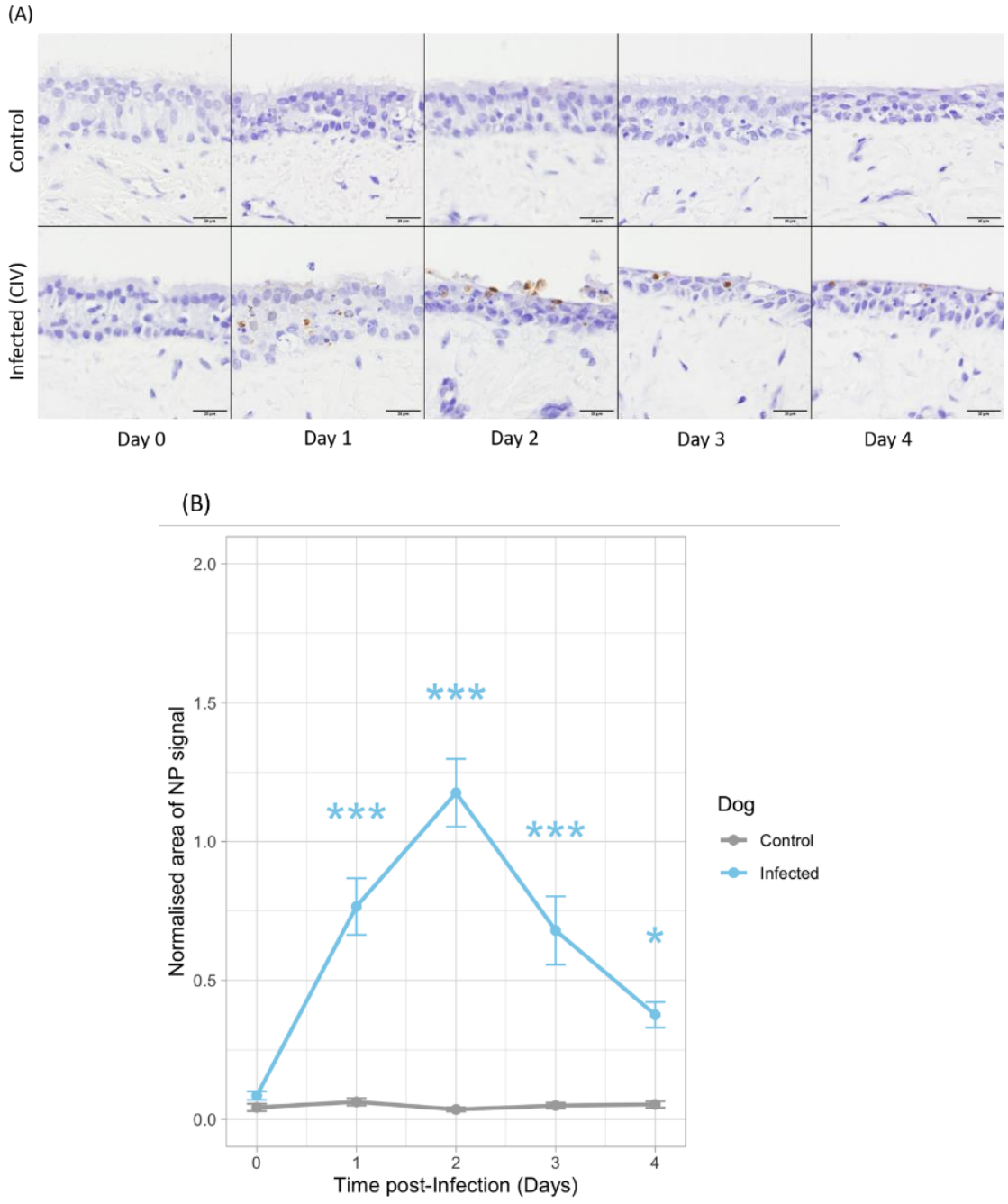

Figure 11. Representative microphotographs (A) and quantification of NP expression (B) in canine tracheal explants. Control and CIV infected explants, representative images at 0, 1, 2, 3, and 4 dpi, NP (A). Quantification of NP expression, measured in pixels, in canine control and CIV infected explants. Point estimates are means and bars are standard errors of the mean. Significance levels are shown as *** $p<0.001$, ** $p<0.01$, and * $p<0.05$ (B).

3.3.2.2. Swine explants

The peak of NP expression in SIV-infected explants was observed at 3 dpi, to then decrease at 4 dpi. Whereas there was a trend towards NP expression at 1 and 2 dpi, differences between control and SIV infected samples were not statistically significant ($p \geq 0.5$). Statistically highly significant ($p<0.001$) differences were seen between control and SIV infected explants at 3 and 4 dpi (multivariate GLM test) (Figure 12).

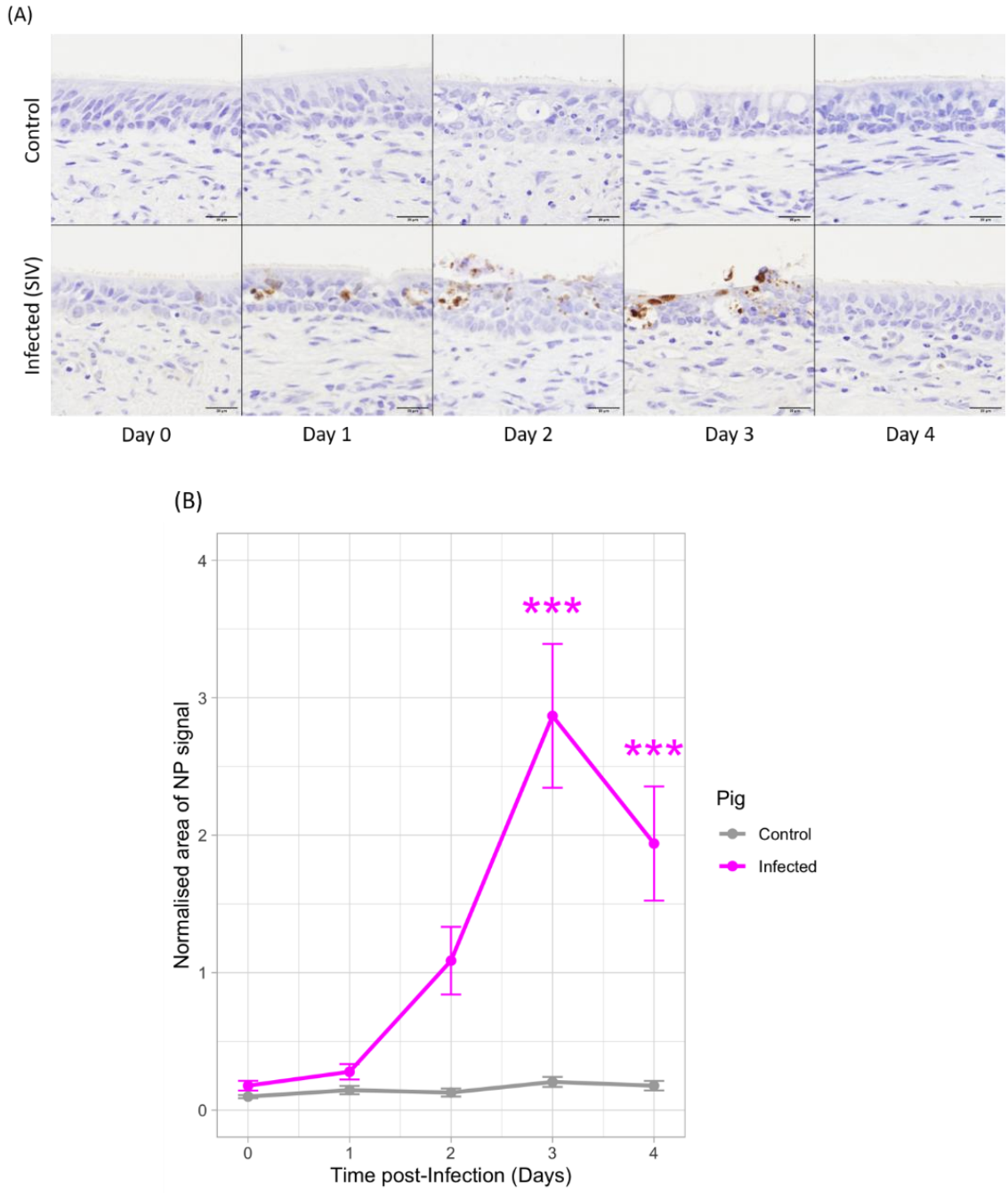

Figure 12. Representative microphotographs (A) and quantification of NP expression (B) in swine tracheal explants. Control and SIV infected explants, representative images at 0, 1, 2, 3, and 4 dpi, NP (A). Quantification of NP expression, measured in pixels, in swine control and SIV infected explants. Point estimates are means and bars are standard errors of the mean. Significance levels are shown as *** $p<0.001$, ** $p<0.01$, and * $p<0.05$ (B).

3.3.3. Quantification of CC3 expression

CC3 was quantified in a total of 270 pictures from canine explants and 270 pictures from swine explants. The total number of positive pixels was normalised by the area of the epithelium.

Both species displayed increased trend on CC3 expression in the infected explants compared with the control ones and showed a peak of expression at 4 dpi. Nevertheless, differences between CIV- or SIV-infected and control explants were not statistically significant ($p \geq 0.5$) (multivariate GLM test) (Figures 13 & 14).

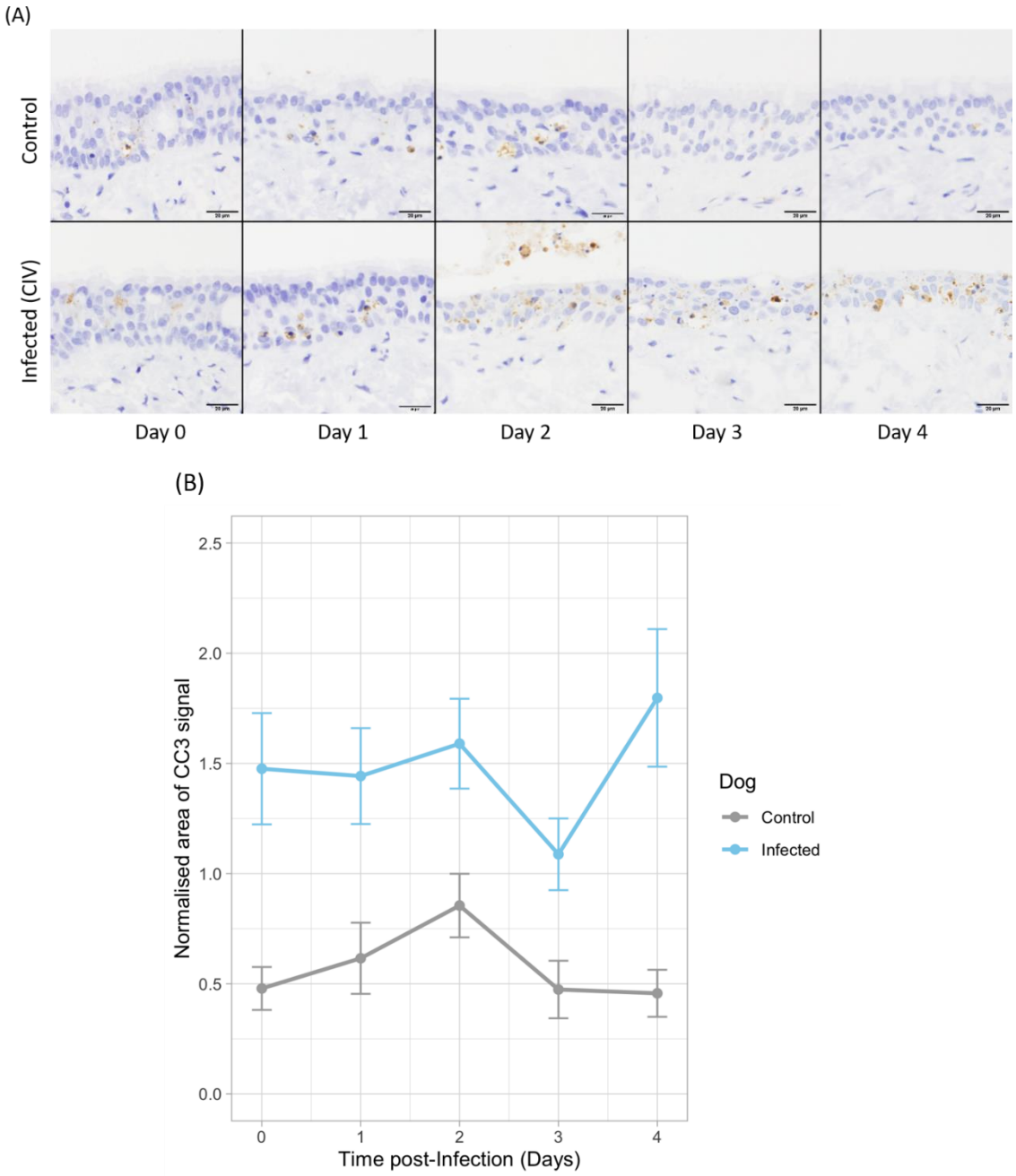

Figure 13. Representative microphotographs (A) and quantification of NP expression (B) in canine tracheal explants. Control and CIV infected explants, representative images at 0, 1, 2, 3, and 4 dpi, CC3 (A). Quantification of CC3 expression, measured in pixels, in canine control and CIV infected explants. Point estimates are means and bars are standard errors of the mean. Significance levels are shown as *** $p<0.001$, ** $p<0.01$, and * $p<0.05$ (B).

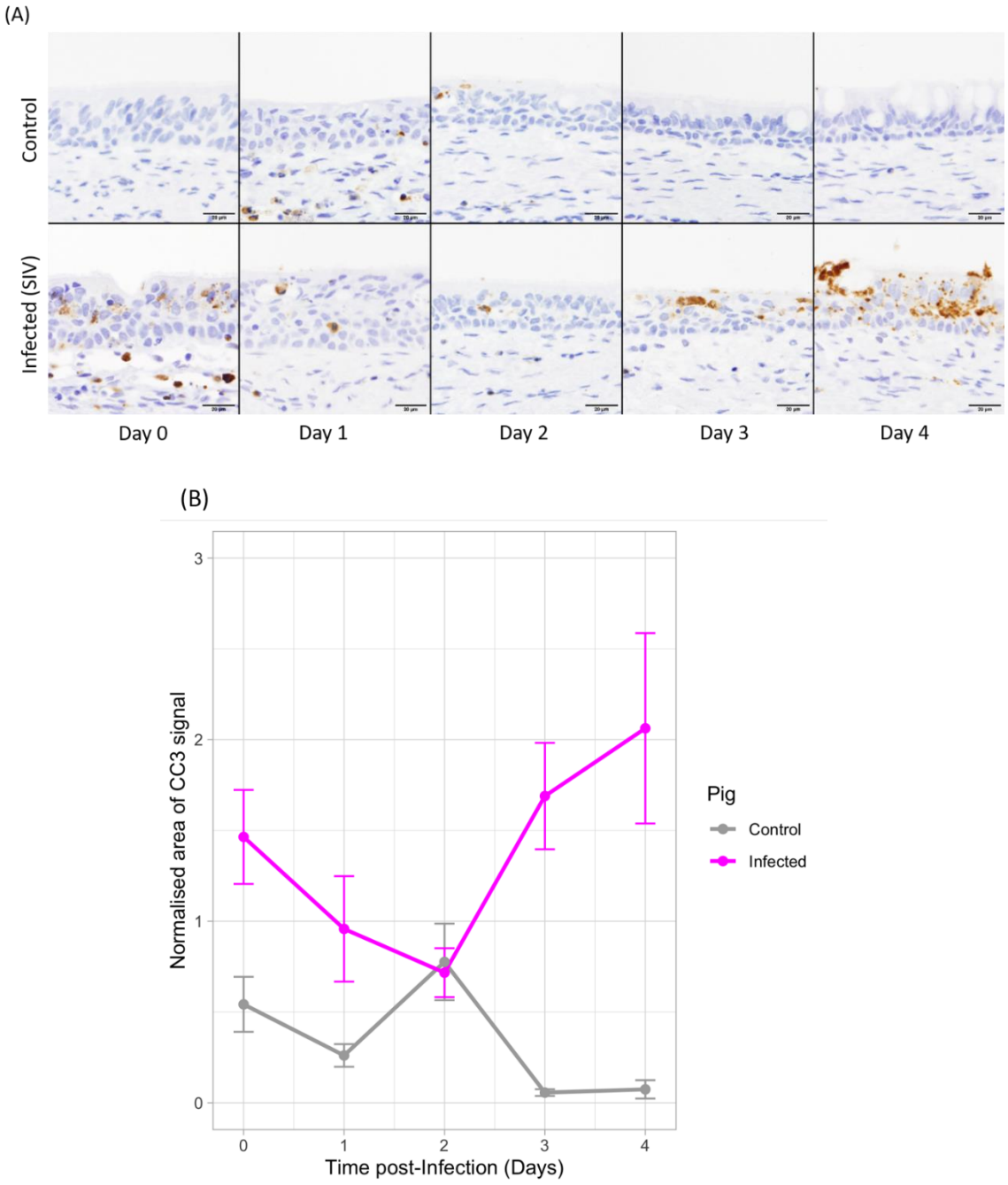

Figure 14. Representative microphotographs (A) and quantification of CC3 expression (B) in swine tracheal explants. Control and SIV infected explants, representative images at 0, 1, 2, 3, and 4 dpi, CC3 (A). Quantification of CC3 expression, measured in pixels, in swine control and SIV infected explants. Point estimates are means and bars are standard errors of the mean. Significance levels are shown as *** $p<0.001$, ** $p<0.01$, and * $p<0.05$ (B).

3.3.4. Quantification of MX1 expression

Mx1 expression was quantified in 246 pictures from canine explants and 267 pictures from swine explants, and the total number of pixels was normalised by the area of the epithelium. Mx1 expression was also expected to be present in control explant.

3.3.4.1. Canine explants

Mx1 showed the peak of expression at 4 dpi in CIV-infected explants, with a progressive increase from day 0 to day 4 post infection. Despite Mx1 expression being also present in control explants, it was still at lower levels compared with the CIV infected samples (Figure 12). Significant statistically ($p<0.001$) differences were observed between control and CIV infected explants at 2 and 3 dpi, and 4 dpi ($p<0.01$) (non-parametric Wilcoxon Mann Whitney test) (Figure 15).

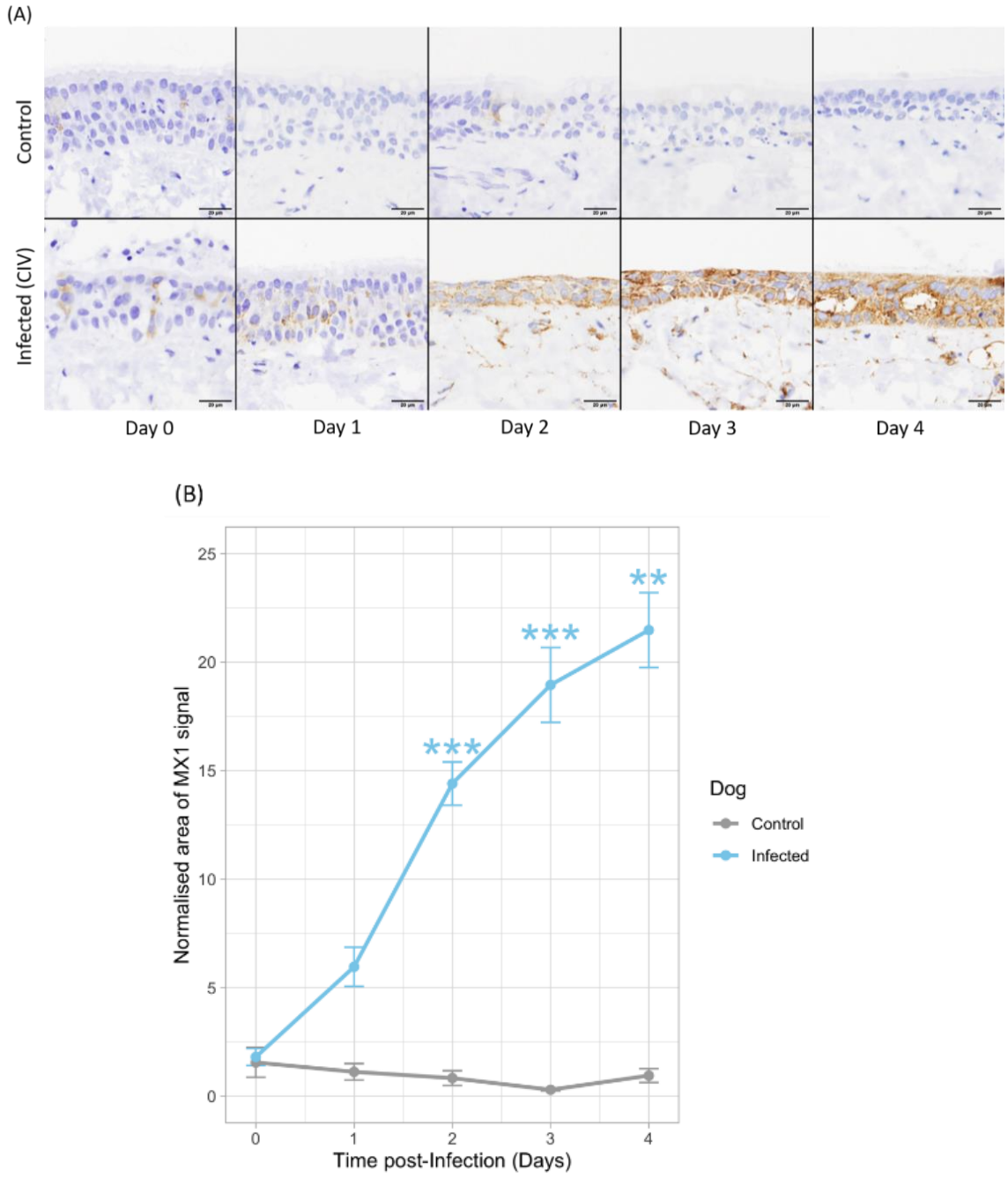

Figure 15. Representative microphotographs (A) and quantification of Mx1 expression (B) in canine tracheal explants. Control and CIV infected explants, representative images at 0, 1, 2, 3, and 4 dpi, Mx1 (A). Quantification of Mx1expression, measured in pixels, in canine control and CIV infected explants. Point estimates are means and bars are standard errors of the mean. Significance levels are shown as *** p<0.001, ** p<0.01, and * p<0.05 (B).

3.3.4.2. Swine explants

The peak of Mx1 expression in swine explants infected with SIV was also at 4 dpi; however, it showed an increased expression at 0 dpi to then decrease at 1 and 2 dpi, to finally increase progressively from day 2 to day 4 post infection. Similar to canine explants, Mx1 positive staining was also observed in control explants of pigs, nevertheless at significantly lower levels compared to the SIV infected samples (Figure 16). Statistically significant ($p<0.01$) and highly significant ($p<0.001$) differences were seen between control and SIV infected explants at 3 and 4 dpi respectively (non-parametric Wilcoxon Mann Whitney test) (Figure 16).

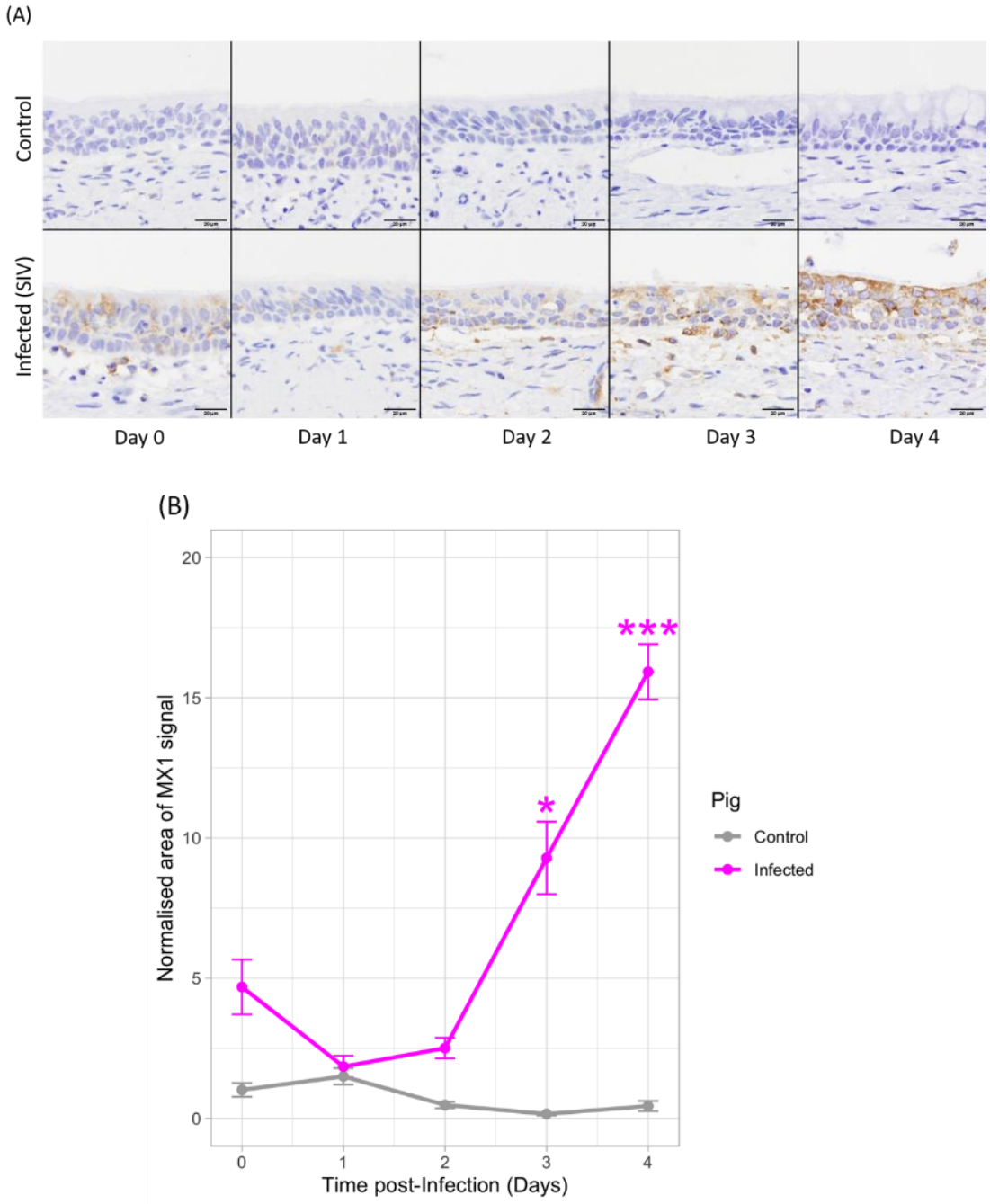

Figure 16. Representative microphotographs (A) and quantification of Mx1 expression (B) in swine tracheal explants. Control and SIV infected explants, representative images at 0, 1, 2, 3, and 4 dpi, Mx1 (A). Quantification of Mx1expression, measured in pixels, in swine control and SIV infected explants. Point estimates are means and bars are standard errors of the mean. Significance levels are shown as *** p<0.001, ** p<0.01, and * p<0.05 (B).

3.3.5. Challenges in quantification of ki67 expression in swine explants

Different limitations were identified while trying to quantify ki67 expression in swine explants using Image J software. The aim of quantifying ki67 signal in tracheal explants was to assess the number of cells in a proliferative stage (G1, S, G2, and mitosis) over the total number of cells in the field, and generate a percentage. The first issue was that the software measured positive stain without separating it by different cells (Figure 17, A&B). Several positive nuclei in close proximity were counted as a single positive area (and thus as a single cell), and therefore, the total number of positive cells in the field was not obtained.

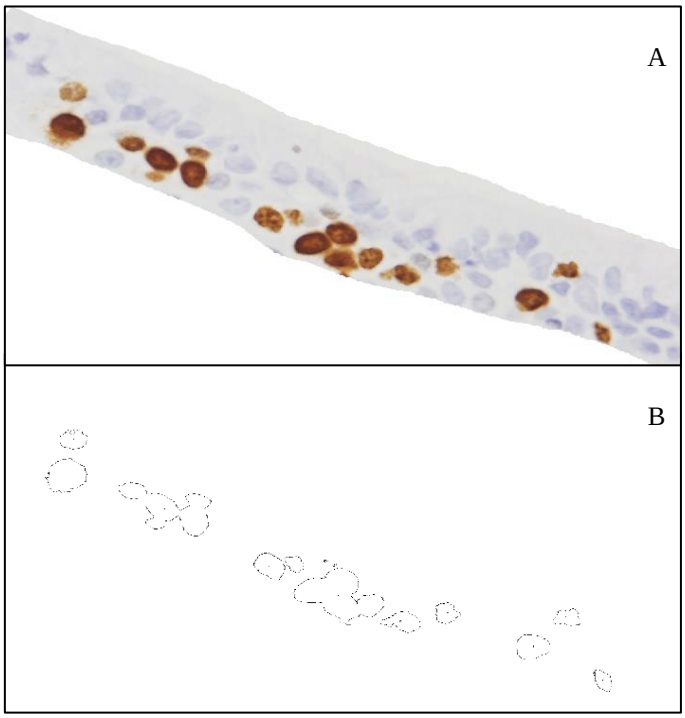

Figure 17. Representative microphotograph of ki67 (A) and quantified positive signal of the same sample (B) in a swine tracheal explant. Ki67 expression was exclusively nuclear with a gradient of expression (from faint to strong) (A). Quantified ki67-positive nuclei were clustered in a single total area for many cells in proximity.

A second challenge was the presence of a single positive cell counted as multiple individual cells, since the staining was not always homogeneous and different dots were identified as positive signals in the same cell.

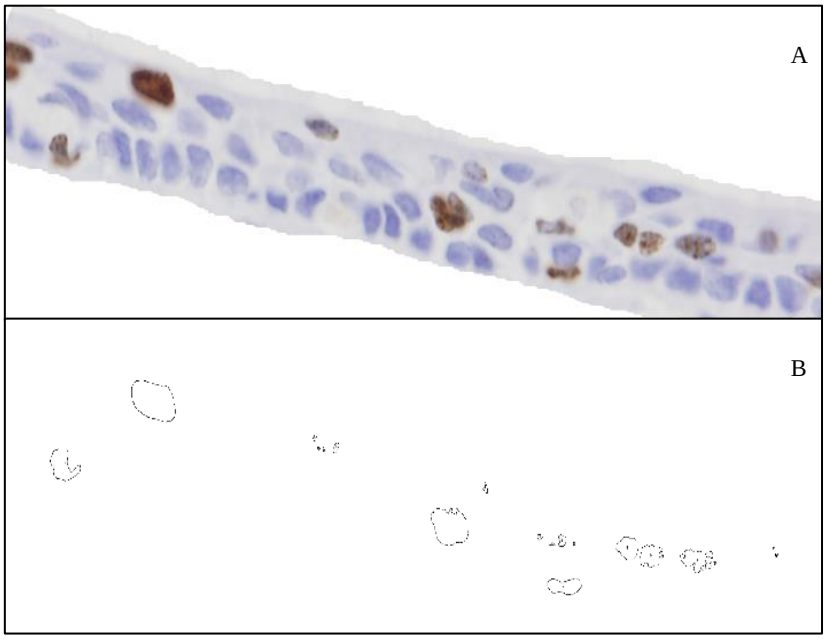

Figure 18. Representative microphotograph of ki67 (A) and quantified positive signal of the same sample (B) in a swine tracheal explant.

Ki67 expression was exclusively nuclear with a gradient of expression (from faint to strong) and revealed a clamped pattern (A). Quantified ki67-positive expression was counted as multiple positive cells within the same cell.

4. Discussion and Conclusions

The overarching objective of this project was to explore the possibility of quantifying pathology using an unbiased method as an attempt to reduce subjectivity from the pathologist's eye. Histopathological analysis can be applied to either naturally occurring or experimentally induced diseases. Especially in experimental studies, the assessment of presence/absence of pathological changes can be considered insufficient, and a method for quantification and scoring of the changes is needed, to be able to highlight differences amongst the studied groups and therefore define the extension of the pathological process.

An accurate definition of the severity of the lesions using grading and scoring provides reliable understanding of the pathophysiology of a disease and accurate definition of the therapeutic management and/or prophylaxis of the disease. Histopathological scoring/grading also enables statistical analysis of phenotype or treatment effects, to more accurately answer scientific questions (Treuting & Boyd, 2019). However, traditional histopathological scoring reveals several limitations, as it only provides a semiquantitative analysis and two independent trained pathologists should perform the assessment in a blind approach. Whilst a blind analysis is recommended to eliminate bias, it is also considered critical that the pathologist has full details of the study to provide the most robust and valid data questions (Treuting & Boyd, 2019).

New technologies for digital image analysis offer the possibility to overcome the limitations of traditional histopathology scoring systems and provide reproducible data that can be further assessed by statistical analysis. This allows to convert pathological analysis into quantifiable parameters (Grant Maxie & Miller, 2016). The role of the pathologist remains crucial to set up the software and interpretate and validate the obtained data.

For this study, a freely downloadable image analysis software (Image J) developed at the National Institutes of Health and the Laboratory for Optical and Computational Instrumentation (LOCI, University of Wisconsin) was used, which was firstly released in 1997 (Schneider, et al., 2012) (Collins, 2007). This software was employed to assess *ex vivo* organ culture tracheal explants of dogs and pigs infected with CIV and SIV,

respectively, to understand the pathogenesis of this disease and define the timepoints of the histopathological changes in the trachea caused by these viruses.

A traditional histological approach of the H&E samples to detect the morphological changes induced by the virus was firstly carried out, in order to assess the good quality of the selected system and determinate the specific histopathological changes to focus on and would be subsequently quantified.

Compared with the control (non-infected) samples, different changes were attributed to CIV and SIV infection. The findings were consistent with loss of cilia and cells (ciliated epithelium and Goblet cells), epithelial degeneration, and regeneration. The histopathological changes noted in my samples were similar to what has been described in tracheas of dogs and pigs infected with CIV and SIV, respectively (Janke, 2014) (Watson, et al., 2017).

The most striking microscopic change was reduction of the epithelial area/thickness, most likely resulting from loss of the outer epithelial cellular layer and reduction in the number of Goblet cells.

Different microscopic changes were attributed to cellular degeneration, represented by attenuation and flattening of superficial epithelial cells, occasional epithelial vacuolation, karyorrhexis, and increased number of apoptotic cells.

Regeneration was recognised as an increase in mitotic figures throughout the full thickness mucosa and not only restricted to the basal layer.

The main shortcoming of this EVOC system is the lack of systemic responses (e.g. inflammation), as recruitment of cells of the immune system to the infection site is abrogated (Bieniasz, 2004). However, this could be seen as an advantage when studying the tissue response to infection in isolation (innate and intrinsic immunity) (e.g. the IFN-mediated response). Another limitation could be a relatively short life span of the explants, usually ranging from 60 hours to 5 days (Glorieux, *et al.*, 2007). Therefore, this study was based on up to 4 days post infection.

The main difference between *in vivo* systems and the samples in this study was the absence of inflammation and haemorrhage, considering the *ex vivo* nature of the samples used in this thesis (Lyoo, et al., 2014) (Zeng, et al., 2013). Loss of ciliated epithelial cells

and Goblet cells was evident in both the *in vivo* models and the *ex vivo* model used in this thesis, and in both represented the earliest sign attributable to CIV and SIV infection. Compared to results of this thesis, epithelial regeneration has not been largely described in the trachea of *in vivo* experiments; however it has been largely described in *in vivo* models of horses infected with equine influenza virus (EIV) (Muranaka, et al., 2012).

Taking into account the changes found in the first traditional assessment of the samples, immunohistochemistry analyses were used to investigate and quantify viral infection/spread (NP), apoptosis (CC3), innate immunity (MX1), and regeneration (ki67).

The first goal was to correlate the evidence of pathological changes to the effective presence of the virus. For this purpose, an antibody directed against NP was employed to detect viral antigen, similarly to what has been described by Gonzalez in canine explants (Gonzalez, et al., 2014) and Nunes in swine explants (Nunes et al., 2010). NP is primarily implicated in nuclear targeting and plays its role when the virus has already entered into the cell, for this reason, it suits best to investigate the spread of the infection in terms of viral replication. NP was evident in well preserved and degenerate epithelium, and was restricted to CIV- and SIV-infected samples.

Given the apparent increased numbers of mitotic figures in the H&E sections of CIV and SIV infected explants, an immunohistochemistry technique was applied to further investigate apoptosis. Additionally, it has been reported that influenza A virus evokes both apoptosis and necroptosis *in vitro* and *in vivo* models (Nogusa, et al., 2016). CC3 is an easily available IHC marker for the study of apoptosis, and the changes seen on H&E by visual microscopic investigation of the samples (shrinkage, nuclear condensation, hyerpeosinophilia) were more consistent with apoptosis rather than necroptosis (cellular swelling as the main feature). Regardless of the pathway of activation (intrinsic or extrinsic), caspase-3 represents one of the executioner caspases and once cleaved the cell is irremediably committed to die (Robbins, et al., 2005). Therefore, CC3 was particularly beneficial to detect early stages of apoptosis, otherwise microscopically unapparent. CC3 was evident in the nuclei of shrunken epithelial cells throughout the epithelium and in cellular fragments of dead cells present in the tracheal lumen.

Ki 67 was used to highlight and analyse regeneration. Ki67 is a nuclear protein expressed in cycling cells in all the active phases, with expression restricted to the nucleus (Vascellari, et al., 2012). In pig-derived explants, ki67 expression was exclusively present

in the nuclei of epithelial cells scattered throughout the full-thickness epithelium in infected samples, with a staining pattern ranging from weakly stippled to strong and homogeneous. On the contrary, in control (non-infected) samples, ki67 expression was restricted to the basal layer of the epithelium, which was already expected as a physiologic process since basal cells are responsible for repopulating the epithelium. For canine explants, ki67 staining appeared very weak with clearly identifiable mitotic figures lacking any ki67 signal, despite attempts with different antibody concentrations (1:200 and 1:500). Therefore, ki67 expression was not considered a trustable marker in my canine samples, and its use in this species was eventually not studied.

Finally, innate immunity was considered an important factor to assess whether it would be increased in infected explants compared to non-infected ones. In other words, to understand if there was a response of the tissue against the virus. Mx1 was chosen for this purpose. Mx1 is a well-known protein considered to be a host restriction factor of the innate immunity system against influenza A viruses (Fatima, et al., 2019). As expected, Mx1 expression was restricted to the cytoplasm of epithelial cells and increased variably in both CIV- and SIV-infected explants compared to control samples.

As previously stated in this thesis, quantification of these parameters was assessed with Image J software, using 3 images per slide from areas selected by this author and considered most representative of the sample. Given the size of the samples and that the chosen areas were manually selected, 3 images per slide was considered accurate to represent the characteristic features of the sample.

NP quantification demonstrated a peak of infection at 2 dpi in dogs, whereas pigs showed it at 3 dpi, to progressively decrease. Statistically significant differences were present between control and infected canine and swine explants. These results suggest that the progression of CIV infection may occur more acutely than SIV.

As expected, in dogs, the epithelial area was particularly decreased at day 2 post-infection and was statistically significant. This also correlates with the peak of NP expression at this time of infection (2dpi) in this species. Interestingly, swine explants infected with SIV showed a decrease in the epithelial area at 3 and 4 dpi, but these findings were not statistically significant compared to control animals. These results could be interpreted as that the epithelial loss is not a significant finding in pigs infected with SIV; however Nunes et al. previously reported a significant difference in the thickness of the epithelium

between SIV-infected and control swine explants, with marked reduction at day 1 post-infection (Nunes, et al., 2010). These differences might be due to the different SIV strains used by Nunes and Patrono (this study).

Quantification of CC3 expression in both species showed the highest peak at 4 dpi; however, differences between mock and infected explants were not statistically significant. The increase in CC3 expression following SIV and CIV infection may suggest that apoptosis could be one of the mechanisms for virus removal and acceleration of infection resolution in this model. Whilst differences between mock and infected explants were not statistically significant in my study, apoptosis induced during influenza virus infection has been broadly considered as a major contributing factor to cell death and tissue damage (Tran, et al., 2013). Therefore, it was considered that, whilst statistical analysis indicates these changes may not be significant, a trend in an increase in the number of CC3-positive cells could be sufficient to include apoptosis as a key mechanism of cell death in CIV and SIV infected dogs and pigs, respectively. Culture conditions need to be also considered as a potential factor producing changes in the morphology of the tissues.

MX1 expression revealed a peak of expression at 4 dpi in both canine and swine infected explants, with statistically significant differences between mock and infected samples. Therefore, and also taking into account that MX1 has been proved to play a significant role in response to Influenza virus infections, the higher expression in infected explants is considered definitely attributed to influenza A infection. The presence of low MX1 expression in mock explants might suggest basal activity as a protective source to the animal against possible infectious/irritant agents.

After the limitation of poor staining of canine explants with ki67 (as previously discussed), a second limitation was noted when quantifying ki67 expression in swine explants. Image J measured positive staining without separating it by different cells, and different positively stained cells that clumped together were counted as a single one, and therefore it was not possible to quantify the total number of positive cells in the field. Additionally, the positive signal was not always homogeneous, commonly showing a clumped expression. These multiple positive dots within the same cell were counted as multiple positive cells. Taking into account all these challenges with ki67 expression,

quantification of the expression of this staining was not included, since it was not considered accurate enough to get robust results.

In conclusion, it is considered by this author that quantification of pathological changes associated with infection of CIV and SIV in canine and swine tracheal explants, respectively, is a feasible and unbiased method, which can be statistically analysed and suitable for a more accurate time-dependent study of the disease than the traditional microscope view.

Overall, the changes seen during the traditional visual microscopic assessment correlated with the results obtained using Image J; however, Image J was able to give a more accurate overview of the pathological changes depending on time post-infection, and allowed statistical analysis of the data.

Whilst quantification of the epithelial thickness, NP, CC3, and MX1 expression was considered to be accurate and feasible in this system, in the case of ki67, Image J was not considered to be reliable enough, and a manual assessment would still need to be performed in order to quantify positive cells, and therefore quantification of regeneration. Other image analyses softwares could be investigated in the future to assess whether these can overcome this issue.

Additionally, these results also open the possibility to consider using similar quantification analyses in other diseases. Image analysis has already been used for quantifying other lesions, such as myocardial fibrosis (Daunoravicius, et al., 2014), or renal pathology (Rangan & Tesch, 2007), and new technology and image analysis software are likely to provide new possibilities for research and grading of diseases.

The figure of the pathologist, however, should, in my opinion, remain essential in all the steps of the analysis, including selection of the experiment, training of the software, first assessment of samples, and interpretation of the results.

5. References

Bieniasz PD. (2004). Intrinsic immunity: a front-line defence against viral attack. *Nat Immunol.* Nov;5(11):1109-15.

Caswell, JL & William, KJ. (016). Respiratory System. In Jubb, Kennedy, and Palmer's, Pathology of Domestic Animals (Vol. 2; p. 567). Elsevier.

Centers for Disease Control and Prevention. (2022). Influenza Type A Viruses [online]. Available from: https://www.cdc.gov/flu/avianflu/influenza-a-virussubtypes.htm#Subtypes [accessed 1 December 2023]

Chambers TM, Balasuriya UB, Reedy SE, Tiwari A. (2013). Replication of avian influenza viruses in equine tracheal epithelium but not in horses. *Influenza and Other Respiratory Viruses 7* (Suppl. 4), 90–93.

Chan RW, Chan MC, Nicholls JM, Malik Peiris JS. (2013). Use of *ex vivo* and *in vitro* cultures of the human respiratory tract to study the tropism and host responses of highly pathogenic avian influenza A (H5N1) and other influenza viruses. *Virus Res.* Dec 5;178(1):133-45.

Collins TJ. (2007). ImageJ for microscopy. *Biotechniques.* Jul;43(1 Suppl):25-30.

Cox NJ, Trock SC, Uyeki TM. (2017). Public Health implications of animal influenza viruses. In Animal Influenza (Chapter 5; p 92). Wiley Blackwell

Crawford PC, Dubovi EJ, Castleman WL, Stephenson I, Gibbs EP, Chen L, Smith C, Hill RC, Ferro P, Pompey J, Bright RA, Medina MJ, Johnson CM, Olsen CW, Cox NJ, Klimov AI, Katz JM, Donis RO. (2005). Transmission of equine influenza virus to dogs. *Science.* Oct 21;310(5747):482-5.

Daunoravicius D, Besusparis J, Zurauskas E, Laurinaviciene A, Bironaite D, Pankuweit S, Plancoulaine B, Herlin P, Bogomolovas J, Grabauskiene V, Laurinavicius A. (2014). Quantification of myocardial fibrosis by digital image analysis and interactive stereology. *Diagn Pathol.* Jun 9;9:114.

Detmer SE. (2017). The clinical features, pathobiology, and epidemiology of influenza infections in pigs. In Animal Influenza (Chapter 16; p 444). Wiley Blackwell

Fatima U, Zhang Z, Zhang H, Wang XF, Xu L, Chu X, Ji S, Wang X. (2019). Equine Mx1 Restricts Influenza A Virus Replication by Targeting at Distinct Site of its Nucleoprotein. *Viruses.* Dec 2;11(12):1114.

Fu Y, Dürrwald R, Meng F, Tong J, Wu NH, Su A, Yin X, Haas L, Schmidtke M, Zell R, Krumbholz A, Herrler G. (2019). Infection Studies in Pigs and Porcine Airway Epithelial Cells Reveal an Evolution of A(H1N1)pdm09 Influenza A Viruses Toward Lower Virulence. *J Infect Dis.* Apr 19;219(10):1596-1604.

Glorieux S, Van den Broeck W, van der Meulen KM, Van Reeth K, Favoreel HW, Nauwynck HJ. (2007). In vitro culture of porcine respiratory nasal mucosa explants for studying the interaction of porcine viruses with the respiratory tract. *J Virol Methods.* Jun;142(1-2):105-12.

Gonzalez G, Marshall JF, Morrell J, Robb D, McCauley JW, Perez DR, Parrish CR, Murcia PR. (2014). Infection and pathogenesis of canine, equine, and human influenza viruses in canine tracheas. *J Virol.* Aug;88(16):9208-19.

Gown AM, Willingham MC. (2002). Improved detection of apoptotic cells in archival paraffin sections: immunohistochemistry using antibodies to cleaved caspase 3. *J Histochem Cytochem.* Apr;50(4):449-54.

Grant Maxie M, Miller MA. (2016). Introduction to the Diagnostic Process. In Jubb, Kennedy, and Palmer's, Pathology of Domestic Animals (Vol. 1; p. 3). Elsevier.

Horai Y, Mizukawa M, Nishina H, Nishikawa S, Ono Y, Takemoto K, Baba N. (2019). Quantification of histopathological findings using a novel image analysis platform. J *Toxicol Pathol.* Oct;32(4):319-327.

Howley, PM, Knipe, DM, Whelan, S & Ovid Technologies Inc. (2021). Fields virology. Volume 1, Emerging viruses. 7th ed. Philadelphia: Wolters Kluwer.

Hui KPY, Cheung MC, Perera RAPM, Ng KC, Bui CHT, Ho JCW, Ng MMT, Kuok DIT, Shih KC, Tsao SW, Poon LLM, Peiris M, Nicholls JM, Chan MCW. (2020). Tropism, replication competence, and innate immune responses of the coronavirus SARS-CoV-2 in human respiratory tract and conjunctiva: an analysis in *ex vivo* and *in vitro* cultures. *Lancet Respir Med*. Jul;8(7):687-695.

International Committee on Taxonomy of Viruses. (2011). Orthomyxoviridae - Negative Sense RNA Viruses - Negative Sense RNA Viruses [online]. Available from: https://talk.ictvonline.org/ictv-reports/ictv_9th_report/negative-sense-rna-viruses-

Janke BH. (2014). Influenza A virus infections in swine: pathogenesis and diagnosis. *Vet Pathol*. Mar;51(2):410-26.

Kang YM, Kim HM, Ku KB, Park EH, Yum J, Seo SH. (2013). H3N2 canine influenza virus causes severe morbidity in dogs with induction of genes related to inflammation and apoptosis. *Vet Res*. Oct 3;44(1):92.

Larson LJ, Henningson J, Sharp P, Thiel B, Deshpande MS, Davis T, Jayappa H, Wasmoen T, Lakshmanan N, Schultz RD. (2011). Efficacy of the canine influenza virus H3N8 vaccine to decrease severity of clinical disease after cochallenge with canine influenza virus and Streptococcus equi subsp. zooepidemicus. *Clin Vaccine Immunol.* Apr;18(4):559-64.

Lee C, Song D, Kang B, Kang D, Yoo J, Jung K, Na G, Lee K, Park B, Oh J. (2009). A serological survey of avian origin canine H3N2 influenza virus in dogs in Korea. *Vet Microbiol*. Jun 12;137(3-4):359-62.

Lyoo KS, Kim JK, Jung K, Kang BK, Song D. (2014). Comparative pathology of pigs infected with Korean H1N1, H1N2, or H3N2 swine influenza A viruses. *Virol J.* Sep 24;11:170.

Maglennon GA, Murphy S, Adams V, Miller J, Smith K, Blunden A, Scase TJ. (2008). Association of Ki67 index with prognosis for intermediate-grade canine cutaneous mast cell tumours. *Vet Comp Oncol*. Dec;6(4):268-74.

Muranaka M, Yamanaka T, Katayama Y, Niwa H, Oku K, Matsumura T, Oyamada T.(2012). Time-related Pathological Changes in Horses Experimentally Inoculated with Equine Influenza A Virus. *J Equine Sci*. 23(2):17-26.

Nogusa S, Thapa RJ, Dillon CP, Liedmann S, Oguin TH 3rd, Ingram JP, Rodriguez DA, Kosoff R, Sharma S, Sturm O, Verbist K, Gough PJ, Bertin J, Hartmann BM, Sealfon SC, Kaiser WJ, Mocarski ES, López CB, Thomas PG, Oberst A, Green DR, Balachandran S. (2016). RIPK3 Activates Parallel Pathways of MLKL-Driven Necroptosis and FADD-

Mediated Apoptosis to Protect against Influenza A Virus. *Cell Host Microbe.* Jul 13;20(1):13-24.

Nunes SF, Murcia PR, Tiley LS, Brown IH, Tucker AW, Maskell DJ, Wood JL. (2010). An *ex vivo* swine tracheal organ culture for the study of influenza infection. *Influenza Other Respir Viruses.* Jan;4(1):7-15.

Park M, Wu P, Goldstein E, Joo Kim W, Cowling BJ. (2015). Influenza-Associated Excess Mortality in South Korea. *Am J Prev Med*. Apr;50(4):e111-e119.

Parrish CR, Dubovi EJ. (2017). Canine Influenza. In Animal Influenza (Chapter 22; p 551). Wiley Blackwell

Parrish CR, Voorhees IEH. (2019). H3N8 and H3N2 Canine Influenza Viruses: Understanding These New Viruses in Dogs. *Vet Clin North Am Small Anim Pract*. Jul;49(4):643-649.

Patrono LV, Bonfante F, Zanardello C, Terregino C, Capua I, Murcia PR. (2015). Phylogenetically distinct equine influenza viruses show different tropism for the swine respiratory tract. *J Gen Virol.* May;96(Pt 5):969-974.

Rangan GK & Tesch GH, (2007). Quantification of renal pathology by image analysis. *Nephrology (Carlton).* Dec;12(6):553-8.

Richt JA, Lager KM, Janke BH, Woods RD, Webster RG, Webby RJ. (2003). Pathogenic and antigenic properties of phylogenetically distinct reassortant H3N2 swine influenza viruses cocirculating in the United States. *J Clin Microbiol*. Jul;41(7):3198-205.

Robbins SL, Cotran RS, Kumar V, Abbas AK, Aster JC. (2005). Cellular Response to Stress and Toxic Insults: Adaptation, Injury, and Death. In: Robbins and Cotran Pathologic Basis of Disease (pp. 52-59). Elsevier.

Russell WMS & Burch RL. (1959) (as reprinted 1992). The principles of humane experimental technique. Wheathampstead (UK): Universities Federation for Animal Welfare.

Saunders-Hastings PR & Krewski D, (2016). Reviewing the History of Pandemic Influenza: Understanding Patterns of Emergence and Transmission. *Pathogens.* Dec 6;5(4):66.

Schmidt RC, Maassab HF, Davenport FM. (1974). Infection by influenza A viruses of tracheal organ cultures derived from homologous and heterologous hosts. *J Infect Dis*. Jan;129(1):28-36.

Schneider CA, Rasband WS, Eliceiri KW. (2012). NIH Image to ImageJ: 25 years of image analysis. *Nat Methods*. Jul;9(7):671-5.

Tran V, Moser LA, Poole DS, Mehle A. (2013). Highly sensitive real-time *in vivo* imaging of an influenza reporter virus reveals dynamics of replication and spread. *J Virol*. Dec;87(24):13321-9.

Treuting PM, Boyd KL. (2019). Histopathological Scoring. *Vet Pathol.* Jan;56(1):17-18.

Turan K, Mibayashi M, Sugiyama K, Saito S, Numajiri A, Nagata K. (2004). Nuclear MxA proteins form a complex with influenza virus NP and inhibit the transcription of the engineered influenza virus genome. *Nucleic Acids Res.* Jan 29;32(2):643-52.

Van Poucke SG, Nicholls JM, Nauwynck HJ, Van Reeth K. (2010). Replication of avian, human and swine influenza viruses in porcine respiratory explants and association with sialic acid distribution. *Virol J.* Feb 16;7:38.

Vascellari M, Giantin M, Capello K, Carminato A, Morello EM, Vercelli A, Granato A, Buracco P, Dacasto M, Mutinelli F. (2012). Expression of Ki67, BCL-2, and COX-2 in canine cutaneous mast cell tumors: association with grading and prognosis. *Vet Pathol*. Jan;50(1):110-21.

Vincent A, Awada L, Brown I, Chen H, Claes F, Dauphin G, Donis R, Culhane M, Hamilton K, Lewis N, Mumford E, Nguyen T, Parchariyanon S, Pasick J, Pavade G, Pereda A, Peiris M, Saito T, Swenson S, Van Reeth K, Webby R, Wong F, Ciacci-Zanella J. (2014). Review of influenza A virus in swine worldwide: a call for increased surveillance and research. *Zoonoses Public Health.* Feb;61(1):4-17.

Watson CE, Bell C, Toohey-Kurth K. (2017). H3N2 Canine Influenza Virus Infection in a Dog. *Vet Pathol*. May;54(3):527-530.

Zeng XJ, Lin Y, Zhao YB, Lu CP, Liu YJ. (2013). Experimental infection of dogs with H3N2 canine influenza virus from China. *Epidemiology and Infection* ;141(12):2595-2603.9